

Modelling Silicate – Nitrate - Ammonium co-limitation of algal growth and the importance of bacterial remineralisation based on an experimental Arctic coastal spring bloom culture study

5 Tobias R. Vonnahme¹, Martial Leroy², Silke Thoms³, Dick van Oevelen⁴, H. Rodger Harvey⁵, Svein Kristiansen¹, Rolf Gradinger¹, Ulrike Dietrich¹, Christoph Voelker³

¹ Department of Arctic and Marine Biology, UiT – The Arctic University of Norway, Tromsø, Norway

² Université Grenoble Alpes, Grenoble, France

³ Alfred-Wegener Institute for Polar and Marine Research, Bremerhaven, Germany

10 ⁴ Department of Estuarine and Delta Systems, NIOZ Royal Netherlands Institute for Sea Research, and Utrecht University, Texel, Yerseke, Netherlands

⁵ Department of Ocean and Earth Sciences, Old Dominion University, Norfolk, USA

Correspondence to: Tobias R. Vonnahme (T.r.vonnahme@gmail.com) and Christoph Voelker (christoph.voelker@awi.de)

15

Abstract. Arctic coastal ecosystems are rapidly changing due to climate warming. This makes modelling their productivity crucially important to better understand future changes. System primary production in these systems is highest during the pronounced spring bloom, typically dominated by diatoms. Eventually the spring blooms terminate due to silicon or nitrogen limitation. Bacteria can play an important role for extending bloom duration and total CO₂ fixation through ammonium regeneration. Current ecosystem models often simplify the effects of nutrient co-limitations on algal physiology and cellular ratios and simplify nutrient regeneration. These simplifications may lead to underestimations of primary production. Detailed biochemistry- and cell-based models can represent these dynamics but are difficult to tune in the environment. We performed a cultivation experiment that showed typical spring bloom dynamics, such as extended algal growth via bacterial ammonium remineralisation, reduced algal growth and inhibited chlorophyll synthesis under silicate limitation, and gradually reduced nitrogen assimilation and chlorophyll synthesis under nitrogen limitation. We developed a simplified dynamic model to represent these processes. Overall, model complexity in terms of the number of parameters is comparable to the phytoplankton growth and nutrient biogeochemistry formulations in common ecosystem models used in the Arctic while improving the representation of nutrient co-limitation related processes. Such model enhancements that now incorporate increased nutrient inputs and higher mineralization rates in a warmer climate will improve future predictions in this vulnerable system.

35

1 Introduction

40 Marine phytoplankton are responsible for half of the CO₂ fixation on Earth (Field et al., 1998; Westberry
et al., 2008). In high latitude oceans, diatoms are an important group contributing 20-40% of the global
CO₂ fixation (Nelson et al., 1995; Uitz et al., 2010). Marine primary production can be bottom-up limited
by light and/or nutrients like nitrogen (N), phosphorous (P), silicon (Si), and iron (Fe). Their availability
is affected by pronounced geographical and seasonal variations (Eilertsen et al., 1989; Loebl et al., 2009;
45 Iversen and Seuthe, 2011; Moore et al., 2013). Arctic coasts are one of the fastest changing systems due
to climate change. Thus, modelling their dynamics is difficult but crucial for predictions of primary
production with climate change (e.g., Slagstad et al., 2015; Fritz et al., 2017; Lannuzel et al., 2020). In
Arctic coastal ecosystems, primary production is typically highest in spring. In spring, previous winter
mixing supplied fresh nutrients and a stratified surface layer with sufficient light is facilitated by
50 increasing temperatures and potentially sea ice melt (Sverdrup, 1953; Eilertsen et al., 1989; Eilertsen and
Frantzen, 2007; Iversen and Seuthe, 2011). With increasing temperatures and runoff, stratification in
coastal Arctic systems is expected to increase (Tremblay and Gagnon, 2009). This will lead to decreased
mixing and nutrient upwelling in autumn and winter and an earlier stratified surface layer in spring, which
may lead to an earlier spring bloom (Tremblay and Gagnon, 2009). However, at the same time,
55 brownification and increased sediment resuspension is already leading to light inhibition in spring, which
may lead to a delayed spring bloom (Opdal et al., 2019). The spring bloom typically consists of chain-
forming diatoms and is terminated by Si or N limitation (Eilertsen et al., 1989; Iversen and Seuthe, 2011).
Zooplankton grazing is typically of low importance for terminating blooms (e.g., Saiz et al., 2013), while
inorganic nutrients are considered to drive bloom termination (Krause et al. 2019, Mills et al. 2018).
60 Heterotrophic bacteria remineralisation of organic matter may supply additional N and Si (Legendre and
Rassoulzadegan, 1995; Bidle and Azam, 1999; Johnson et al., 2007). N regeneration has been described
as a mostly bacteria-related process (Legendre and Rassoulzadegan, 1995), while Si dissolution is mainly
controlled by abiotic dissolution of silica (Bidle and Azam, 1999). Zooplankton may also release some
ammonium and urea after feeding on phytoplankton, but we suggest that this process is likely far less
65 important than bacterial regeneration (e.g. Saiz et al., 2013). Previously measured ammonium excretion
of Arctic mesozooplankton is typically low compared to bacterial remineralization (Conover and
Gustavson, 1999), with the exception for one study in summer in a more open ocean setting (Alcaraz et
al., 2010). In some Arctic systems urea, excreted by zooplankton may be an important N source for
regenerated algae production (Conover and Gustavson, 1999). A warmer climate will increase both
70 bacteria-related remineralisation rates (Legendre and Rassoulzadegan, 1995; Lannuzel et al., 2020) and
abiotic silica dissolution (Bidle and Azam, 1999). However, the magnitude is not well understood.
Phytoplankton blooms may be dominated by a single or a few algal species, often with a similar
physiology during certain phases of the bloom (e.g., Eilertsen et al., 1989; Degerlund and Eilertsen, 2010;
Iversen and Seuthe, 2011). Chain-forming centric diatoms share physiological needs and responses to
75 nutrient limitations (e.g., Eilertsen et al., 1989; von Quillfeldt, 2005) and typically dominate these blooms.
In some Arctic and sub-Arctic areas the Arctic phytoplankton species chosen for this model, *Chaetoceros*
socialis, can be dominant during spring blooms (Rey and Skjoldal, 1987; Eilertsen et al., 1989; Booth et
al., 2002; Ratkova and Wassmann, 2002; von Quillfeldt, 2005; Degerlund and Eilertsen, 2010). Such
spring phytoplankton blooms are accompanied by heterotrophic bacterioplankton blooms also showing

80 typical succession patterns and distinct re-occurring taxa that dominate the community (Teeling et al.,
2012; Teeling et al., 2016). The importance of bacterial nutrient recycling for regenerated production has
been recognized in several ecosystem models (e.g. van der Meersche et al., 2004; Vichi et al., 2007; Weitz
et al., 2015) and algae bioreactor models focusing on nutrient conversions (e.g. Zambrano et al., 2016).
85 However, these models are typically highly simplified or omitted in more sophisticated dynamic multi-
nutrient, quota based models (e.g. Flynn and Fasham, 1997b.; Wassmann et al., 2006; Ross and Geider,
2009). These latter models have been often developed and tuned based on cultivation experiments in
which microbial remineralization reactions were assumed to be absent (e.g. Geider et al., 1998; Flynn,
2001) despite the fact that most algae cultures, likely including Geider et al., (1998) and Flynn (2001) are
90 not axenic. Parameters estimated by fitting axenic models on non-axenic experiments may be misleading,
mostly by an inflated efficiency of DIN uptake. Additional positive effects of bacteria include vitamin
synthesis (Amin et al., 2012), trace metal chelation (Amin et al., 2012), the scavenging of oxidative
stressors (Hünken et al., 2008), and exchange of growth factors (Amin et al., 2015). Especially in the
stationary algal growth phase, Christie-Oleza et al. (2017) found that marine phototrophic cyanobacteria
95 cultures are dependent on heterotrophic bacteria contaminants mainly due to their importance in
degrading potentially toxic DOM exudates and regenerating ammonium. The current study aimed to
bridge the gap between detailed representations of algae physiology and the role of microbial activity in
an accurate way while keeping model complexity low.

Most ecosystem models consider only a single limiting nutrient to control primary production after
Liebig's Law of the minimum (Wassmann et al., 2006; Vichi et al., 2007). Yet we know that nutrient co-
100 limitation is more complex. For example, ammonium and glutamate can inhibit nitrate uptake (Morris,
1974; Dortch, 1990; Flynn et al., 1997), C and N uptake is reduced under Fe limitation, while Si uptake
continues (Werner, 1977; Firme et al., 2003), and the effects on photosynthesis differs for nitrogen and
silicon limitations and for different algal groups (Werner, 1977; Flynn, 2003; Hohn et al., 2009). Complex
interaction models considering intracellular biochemistry (NH₄-NO₃ co-limitation, Flynn et al., 1997),
105 transporter densities and mobility (Flynn et al., 2018), and cell cycles (Si limitation, Flynn, 2001) can
accurately describe these dynamics (Flynn, 2003), but are ultimately too computationally expensive to be
integrated and parameterized in large scale ecosystem models. Some models (Hohn et al., 2009, Le Quéré
et al., 2016) implemented multi-nutrient (Hohn et al., 2009) and heterotrophic bacterial dynamics (Le
Quéré et al., 2016) in Southern Ocean ecosystem models, but have their limitations in representing
110 bacterial remineralisation (Hohn et al., 2009), or ammonium and silicate co-limitations (Le Quéré et al.,
2016). In contrast to Antarctica, DIN is the primary limiting nutrient for phytoplankton growth while iron
is not limiting in most Arctic systems (Tremblay and Gagnon, 2009; Moore et al., 2013).

While simple lab experiments cannot represent all nutrient dynamics found in the environment (e.g. N
excretion by zooplankton), they can focus on the quantitatively most important dynamics, to facilitate the
115 development of simple multi-nutrient models, which are scalable to larger ecosystem models. The present
study investigated the impact of silicate, ammonium - nitrate co-limitation and bacterial nutrient
regeneration on photosynthesis, nitrogen assimilation, and cellular quotas based on data from a culture
based Arctic spring bloom system. The culture consisted of an axenic isolate of *Chaetoceros socialis*,
dominating a phytoplankton net haul of a Svalbard fjord. The cultivation experiment was conducted either
120 under axenic conditions or after inoculation with mostly free-living bacteria cultures, isolated beforehand
from the non-axenic culture. Parametrization and insights from these incubations were then used to

develop and parameterize a simple Carbon quota based dynamic model (based on Geider et al., 1998), aiming to keep the number of parameters, and computational costs as low as possible to allow for its implementation in large-scale ecosystem models.

125 The aims of the study were I) to study the bloom dynamics of a simplified Arctic coastal pelagic system in a culture experiment consisting of one Arctic diatom species and co-cultured bacteria, II) to develop a simple dynamic model representing the observed interactions, and III) to discuss the importance of more complex bloom dynamics for their accurate representation in ecosystem models.

130 We hypothesize that: I) Bacterial regeneration extends a phytoplankton growth period and gross carbon fixation; II) Diatoms continue photosynthesis under silicate limitation at a reduced rate if DIN is available; III) Cultivation experiments are powerful for understanding the major spring bloom dynamics.

2 Methods

2.1 Cultivation experiment

The most abundant phytoplankton species from a net haul (20 μm mesh size) in April 2017 in van Mijenfjorden (Svalbard) *Chaetoceros socialis* was isolated via the dilution isolation method (Andersen et al., 2005) on F/2 medium (Guillard, 1975). Bacteria were isolated on LB-medium (evaluated by Bertani, 2004) Agar plates using the algae culture as inoculum and sequenced at GENEWIZ LLC using the Sanger method and standard 16S rRNA primers targeting the V1-V9 region (Forwards 5'-AGAGTTTGATCCTGGCTCAG -3', Reverse 5'-ACGGCTACCTTGTTACGACTT -3') provided by GENEWIZ LLC for identification via blastn (Altschul et al., 1990). Two strains of *Pseudoalteromonas elyakovii*, a taxon previously isolated from the Arctic (Khudary et al., 2008) and known to degrade algae polysaccharides (Ma et al., 2008) and to excrete polymeric substances (Kim et al., 2016), were successfully isolated and used for the experiments. Before the start of the experiment, all bacteria in the algae culture were killed using a mixture of the antibiotics penicillin and streptomycin. The success was confirmed via incubation of the cultures on LB-Agar plates and bacterial counts after DAPI staining (Porter et al., 1980). The axenic cultures were diluted in fresh F/2 medium lacking nitrate addition (Guillard, 1975) using sterile filtered seawater of Tromsø sound (Norway) as basis. The algae cultures were transferred into 96 200 ml sterile cultivation bottles with three replicates for each treatment. Half of the incubations were inoculated with bacteria cultures (BAC+), while the other half was kept axenic (BAC-). The cultures were incubated at 4 °C and 100 $\mu\text{E m}^{-2} \text{s}^{-1}$ continuous light and mixed 2-3 times a day to keep the algae and bacteria in suspension. We ensured sterile conditions during the experiment by keeping the cultivation bottles closed until sampling. However, endospores may survive the antibiotic treatment in low numbers and start growing especially towards the end of the experiment. Over 16 days three axenic and three BAC+ bottles were sacrificed daily for measurements of chlorophyll a (Chl), particulate organic carbon (POC) and nitrogen (PON), bacterial and algal abundances, nutrients (nitrate, nitrite, ammonium, phosphate, silicate), dissolved organic carbon (DOC), and the maximum quantum yield (QY) of PSII (Fv/Fm) as a measure of healthy photosystems. Due to technical problems not all replicates could be measured on all days and an overview of replication is given in Table S2.

Chlorophyll a was extracted from a GF/F (50 ml filtered at 200 mbar) filter at 4 °C for 12-24 h in 98%
160 methanol in the dark before measurement in a Turner Trilogy™ Fluorometer (evaluated by Jacobsen and
Rai, 1990). POC and PON were measured after filtration onto precombusted (4 h at 450 °C) GF/F
(Whatman) filters (50 ml filtered at 200 mbar), using a Flash 2000 elemental analyser (Thermo Fisher
Scientific, Waltham, MA, USA) and Euro elemental analyser (Hekatech) following the protocol by Pella
and Colombo (1973) after removing inorganic carbon by fuming with saturated HCl in a desiccator.
165 Bacteria were counted after fixation of a water sample for 3-4 h with 2% Formaldehyde (final
concentration), filtration of 25 ml on 0.2 µm pore size Polycarbonate filter, washing with filtered Seawater
and Ethanol, DAPI staining for 7 minutes after Porter et al. (1980), and embedding in Citifluor-
Vectashield (3:1). Bacteria were counted in at least 20 grids under an epifluorescence microscope (Leica
DM LB2, Leica Microsystems, Germany) at 10x100 magnification. In the same sample the average
170 diameter of diatom cells at the start and end of the experiment was measured. Algae were counted in 2ml
wells under an inverted microscope (Zeiss Primovert, Carl Zeiss AG, Germany) at 20x10 magnification
after gentle mixing of the cultivation bottle. Algae cells incorporated in biofilms after day 9 in the BAC+
cultures were counted after sonication in a sonication bath until all cells were in suspension. Nutrient and
DOC samples were sterile filtered (0.2µm) and stored at -20°C before measurements. Nutrients were
175 measured in triplicates after using standard colorimetric on a nutrient analyser (QuAAtro 39, SEAL
Analytical, Germany) using the protocols No. Q-068-05 Rev. 12 for nitrate (detection limit = 0.02 µmol
L⁻¹), No. Q-068-05 Rev. 12 for nitrite (detection limit = 0.02 µmol L⁻¹), No. Q-066-05 Rev. 5 for silicate
(detection limit = 0.07 µmol L⁻¹), and No. Q-064-05 Rev. 8 for phosphate (detection limit = 0.01 µmol L⁻¹).
180 The data were analysed using the software AACE. The nutrient analyzer was calibrated with reference
seawater (Ocean Scientific International Ltd., United Kingdom). Ammonium was measured manually
using the colorimetric method after McCarthy et al., (1977) on a spectrophotometer (Shimadzu UV-1201,
detection limit = 0.01 µmol L⁻¹). Ammonium values > 100 µmol L⁻¹ were removed as outliers caused by
too high filtration pressure. DOC was measured by high temperature catalytic oxidation (HTCO) using a
Shimadzu TOC-5000 total C analyser following methods for seawater samples (Burdige and Homstead,
185 1994). The photosynthetic quantum yield was determined using an Aquapen PA-C 100 (Photon Systems
Instruments, Czech Republic).

Certain factors, such as grazing, settling out of the euphotic zone, and bacterial and algae succession were
not included into the experimental set-up to reduce complexity, and focus on nutrient dynamics. Trace
metals, phosphate, and Vitamin B12 in coastal systems are assumed to be not limiting in Arctic coastal
190 systems and were supplied in excess to the culture medium. Realistic pre-bloom DOC concentrations
were present in the medium as it was prepared with sterilized seawater from the Fjord outside Tromsø
before the onset of the spring bloom (March 2018).

The f-ratio as indication for the importance of regenerated production (Eppley, 1981) was calculated
based on the average PON fixation in the last three days of the experiment (Eq C1). Here, nitrogen
195 assimilation in the BAC- culture was assumed to be based on new (nitrate based) production, while
fixation in the BAC+ experiment was assumed to also be based on regenerated (ammonium based)
production.

2.2 Model structure

200 This section outlines the overall model structure followed by a description of the chosen parametrization approach for each relevant process. Details regarding model equations are provided in the Appendix (Tables A6 and A7) and a schematic representation of the models is given in Figure 1. We used a dynamic cell quota model by Geider et al. (1998) to describe the BAC- experiment (G98). We then extended the G98 model to represent the role of silicate limitation, bacterial regeneration of ammonium, and different kinetics for ammonium and nitrate uptake (EXT) and fitted it to the BAC+ experiment while retaining
205 the parameter values previously estimated for G98.

The Geider et al. (1998) model (G98) describes the response of phytoplankton to different nitrogen and light conditions and is based on both intracellular quotas and extracellular dissolved inorganic nitrogen (DIN) concentrations, allowing decoupled C and N growth (Fig. 1). Within this model, light is a controlling factor on photosynthesis and chlorophyll synthesis. C:N ratios and DIN concentrations control
210 nitrogen assimilation, which is coupled to chlorophyll synthesis and photosynthesis. Chl:N ratios are controlling photosynthesis and chlorophyll synthesis. G98 has been used in a variety of large scale ecosystem models with some extensions representing the actual conditions in the environment or mesocosms (e.g. Moore et al., 2004; Schartau et al., 2007; Hauck et al., 2013). Photoacclimation dynamics in Geider type models have been evaluated as quick and robust (Flynn et al., 2001), while the N-
215 assimilation component has some shortcomings in regard to ammonium-nitrate interactions. The original model of Geider et al. (1998) for C and N was corrected for minor typographical errors (see Ross and Geider, (2009); Appendix Tables A6 A7).

One aim of the study was to develop a model (EXT) with simplified dynamics of nutrient co-limitation, which is suitable for future implementation in coupled biogeochemistry-circulation models. The EXT
220 model keeps all formulations of the G98 and adds dynamics and interactions of silicate, nitrate and ammonium uptake, carbon and nitrogen excretion and bacterial remineralisation (Fig. 1). The aim of the model was to describe the response in photosynthesis, chlorophyll synthesis and nitrogen assimilation with a minimal number of parameters. Hence, dynamics in silicate cycling and bacterial physiology were highly simplified. The limitations of these simplifications and the potential need for more complex models
225 are discussed later.

Silicate uptake was modelled using Monod kinetics after Spilling et al. (2010). The effect of silicate limitation on photosynthesis and chlorophyll synthesis was implemented after findings by Werner (1978), Martin-Jézéquel et al. (2000), and Claquin et al. (2002). Werner (1978) found that silicate limitation can
230 lead to a 80% reduction in photosynthesis and a stop of chlorophyll synthesis in diatoms within a few hours. Hence, we added a parameter for the reduction of photosynthesis under silicate limitation (S_{IPS}) and formulated a stop of chlorophyll synthesis under silicate limitations.

N and Si metabolism have different controls and intracellular dynamics, with N uptake driven by photosynthesis (as P_C^{ref} in G98) and Si mainly linked to algal respiration (Martin-Jezequel et al., 2000). Besides earlier cultivation studies, the reduction of photosynthesis after Si limitation has been shown via
235 photophysiological (inhibited PSII reaction center, Lippemeier et al., 1999) and molecular (down-regulated photosynthetic proteins, Thangaraj et al., 2019) approaches. In general, we assume that nitrogen metabolism is not directly affected by silicate limitation (Hildebrand 2002, Claquin et al., 2002), but we

expect cellular ratios to be affected by reduced photosynthesis and chlorophyll synthesis under Si limitation (Hildebrand, 2002; Gilpin, 2004).

240 The algal respiration term included both respiration and excretion of dissolved organic nitrogen and carbon as a fraction of the carbon and nitrogen assimilated. For testing the importance of DON excretion, we also ran the EXT model without DON excretion (EXT_{-excr}). Dissolved organic nitrogen (DON) was recycled into ammonium via bacterial remineralisation. It was assumed that this process is faster for freshly excreted DON compared to DON already present in the medium. Thus, we implemented a labile

245 DON pool (DON_i) for freshly excreted DON and a refractory (DON_r) DON pool with the respective remineralization rates rem and rem_d . We also assumed that excreted DON and DOC do not coagulate as extracellular polymeric substances (EPS) during the course of the experiment. After Tezuka (1989), net bacterial regeneration of ammonium occurs at DOM C/N molar ratios below 10 and is proportional to bacterial abundances. Higher thresholds up to 29 have been found (e.g., Kirchmann, 2000), but we

250 selected a lower number to stay conservative. DOM C/N ratios are assumed to be proportional to algae C/N ratios (van der Meersche et al., 2004), with algal molar C/N ratios below 10 representing substrate (DOM) molar C/N ratios below 10.5. Hence, we assumed net bacterial ammonium regeneration to occur at molar POC/PON ratios below 10, while higher ratios lead to bacteria retaining more N for growth than they release. Bacteria abundance change was estimated using a simple logistic growth curve as a function

255 of DOM since the number of parameters is low (2) and the fit sufficient for the purpose of modelling algae physiology. Michaelis-Menton kinetics based on bacteria growth on DOM with different labilities kinetics could give a more accurate representation of bacterial growth but would not change the fit of the other model parameters aiming for the best fit of the model output to algal PON, POC, Chl, and DIN. Algal nitrate uptake was modelled after the original model by Geider et al. (1998) and ammonium

260 assimilation was based on the simplified SHANIM model by Flynn and Fasham (1997b), excluding the internal nutrient and glutamine concentrations. Ammonium uptake is preferred over nitrate (lower half saturation constant) and reduces nitrate assimilation if available above a certain threshold concentration of ammonium (Dortch, 1990; Flynn, 1999). Ammonium is the primary product of bacterial regeneration N-compound after remineralization of DON. Nitrification was assumed to be absent, since the bacteria in

265 our experiment are not known to be capable of nitrification.

2.3 Model fitting

The model was based on a set of ordinary differential equations (ODEs) and was written in R. All model equations are provided in the Appendix (Table A6 and A7) and the newest version of the R code is available on GitHub (<https://github.com/tvonnahm/Dynamic-Algae-Bacteria-model>) and the version

270 used in this manuscript archived at zenodo (doi.org:10.5281/zenodo.4459550). The ODEs were solved using the ode function of the deSolve package (Soetart et al., 2010) with the 2nd-3rd order Runge-Kutta method with automated step size control.

The parameters of the G98 model were fitted to the BAC- experiment data and those of the EXT model were fitted to the BAC+ experiment data. The model fitting started with data from day 1 in order to avoid artifacts during acclimation of the cultures after transfer to a new medium. Si and NO_x were not measured

275 at day 1 and the mean of day 0 and day 2 was used. The G98 parameter values were fitted first and retained without changes for the EXT model fitting. The maximum Chl:N ratio (θ_{max}^N), minimum and maximum

N:C ratios (Q_{\min} , Q_{\max}), and irradiance (I) were available as experimental data and needed no further fitting (Table A2). The start values and constraints for the remaining six variables (ζ , R^C , α_{Chl} , n , K_{no_3} , $P^{\text{C}}_{\text{ref}}$, Table A3) were based on model fits of G98 to other diatom cultures in previous studies (Geider 1998, Ross and Geider 2009). The parameters were first fitted manually via graphical comparisons with the experimental data (POC, PON, Chl, DIN, Fig. 5 and 5), and via minimizing the model cost calculated as the root of the sum of squares normalized by dividing the squares with the variance (RMSE Eq. C2, Stow et al., 2009). The initial manual tuning approach allowed control of the model dynamics, considering potential problems with known limitations of the G98 model (e.g. lag phase not modelled; Pahlow, 2005). The manual tuning also allowed obtaining good start parameters for the automated tuning approach and sensitivity/ collinearity analyses, which are sensitive to the start parameters.

After the manual tuning, an automated tuning approach was used to optimize the fits. The automated tuning was done using the FME package (Soetart et al., 2010b), a package commonly used for fitting dynamic and inverse models based on differential equations (i.e., deSolve) to measured data. The automated analyses were based on minimizing the model cost calculated as the sum of squares of the residuals (SSR, Fitted vs measured data). The experimental data were normalized so that all normalized data were in a similar absolute range of values. This involved increasing Chl and PON values by an order of magnitude while decreasing DIN ($\text{NH}_4 + \text{NO}_3$) data by one order of magnitude. The data were not weighted, assuming equal data quality and importance. Prior to the automated fitting, parameters were tested for local sensitivity (SensFun) and collinearity, or parameter identifiability (collin; e.g., Wu et al., 2014). sensFun tests for changes in output variables at each time point based on local perturbations of the model parameter. The sensitivity is calculated as L1 and L2 norms (Soetart et al. 2009; Soetart et al., 2010b). The sensFun output is further used as input for the collinearity, or parameter identifiability analyses. Parameters were considered collinear and not identifiable in combination with a collinearity index higher than 20 (Brun et al., 2001). In this case, only the more sensitive parameter was used for further tuning. Eventually, R^C , K_{no_3} , n , and α_{Chl} were subject to the automated tuning approach using the modfit function, based on minimizing the SSR within the given constraints. Parameters were first fitted using a Pseudorandom search algorithm (Price, 1977) to ensure a global optimum. The resulting parameters were then fine-tuned using the Nelder-Mead algorithm (Soetart et al., 2010b) for finding a local optimum. A model run with the new parameters was then compared to the initial model via graphical comparisons of the model fit to the experimental data, and via the RMSE value.

The parameter values obtained for the G98 fit to the BAC- experiment were retained without changes or further fitting in the EXT model. The additional parameters of the EXT model were then fitted to the BAC+ experimental data (POC, Chl, PON, DIN). The model was only fitted to total DIN, due to the potential uncertainties related to ammonium immobilization in the biofilm, which could be released during filtration and be part of the measured data. In fact, a test run, fitting the EXT model to NO_3 and NH_4 separately lead to a substantially worse overall fit (RMSE=3.49). Otherwise, the data were not weighted. Since the aim of the study was to model the effects of silicate and bacteria on algae growth and not to develop an accurate model for bacteria biomass and silicate concentrations, the parameters μ_{bact} , bact_{max} , K_{si} , and V_{max} were only fitted to the corresponding data (Bacteria, Silicate) prior to fitting the other parameters of the EXT model. Bacterial growth parameters (μ_{bact} , bact_{max}) were fitted to the bacterial growth curve using common bacterial carbon conversion units (20 fg C per cell as described by Lee and Fuhrman, 1987). Silicate related parameters (K_{si} , V_{max}) were constrained by the study of Werner (1978)

320 and fitted to the measured silicate concentrations. The remaining parameters were subject to the tuning
approach described for G98. Ammonium related parameters (K_{nh4} , $nh4_{thres}$) were constrained by measured
ammonium concentrations, and constants available for other diatom taxa described by Eppley et al.
(1969). Remineralization parameters for excreted (rem) and background (rem_d) DOM were constrained
325 by the data with the limitation of $rem > rem_d$, assuming that the excreted DOM is more labile. The
parameters related to the effect of silicate limitation on photosynthesis and chlorophyll production (S_{min} ,
 S_{ips}) were constrained by the study of Werner (1978) and fitted as described for G98. None of the added
parameters were collinear/ unidentifiable or given by the measured data and thus retained for the
automated tuning approach. Eventually, the 15 parameters (Table A3) were fitted against 160 data points
(Table A1).

330 Due to the biofilm formation in the stationary phase of the BAC+ experiment, we tested two additional
modelling approaches representing different dynamics in biofilms: i) DOC coagulation to EPS as part of
the POC pool, which was assumed absent in our EXT model (Schartau et al., 2007), and ii) Increased
DOM excretion in the stationary phase (e.g. Christie-Oleza et al., 2017). However, we suggest that the
photosynthesis reduction term S_{ips} can give very similar model outputs, while being similarly or more
335 sensitive. Thus, we tested the sensitivity of the added parameters of the two extended biofilm models in
comparison to S_{ips} by testing the magnitude of perturbations of S_{ips} needed to reverse the effects of the
added biofilm parameter (Fig. S1-3). The effects could be mostly reversed with similar or less
perturbations of S_{ips} . However, DOC coagulation to EPS can yield in a better overall better fit than S_{ips}
alone. The main effect of the biofilm that we could not model with the available data appears to be
340 ammonium immobilization in the biofilm, potentially by adsorption, accumulation in pockets, or
conversion to ammonia due to the locally reduced pH caused by increased bacterial respiration. Model
stability was estimated by extending the model run for 120 days, to test for unrealistic model dynamics
(Fig. S3).

3 Results

345 3.1 Cultivation experiment

The concentrations of nitrate and silicate declined rapidly over the course of the experiment (Fig. 2). After
eight days, silicate decreased to concentrations below $2 \mu\text{mol L}^{-1}$ a threshold known to limit diatom
dominance in phytoplankton (Egge and Aksnes, 1992), while inorganic nitrogen (nitrate, nitrite, and
ammonium) became limiting ($<0.5 \mu\text{mol L}^{-1}$, POC:PON $>8-9$ DIN:DIP <16) only in the BAC- culture.
350 DIN:DIP ratios far below 16, or DIN concentrations below $2 \mu\text{mol L}^{-1}$ have been described as indication
for DIN limitation (Pedersen and Borum, 1996), as well as POC:PON ratios >9 (Geider and La Roche,
2002). Phosphate was not potentially growth limiting with molar DIN to PO_4 ratios consistently far below
16 (Redfield, 1934) and concentrations around $15 \mu\text{mol L}^{-1}$. Typically, phosphate concentrations below
 $0.3 \mu\text{mol L}^{-1}$ are considered limiting (e.g., Haecky and Andersson, 1999). Regeneration of ammonium
355 and phosphate were important after eight days as seen by increasing concentrations of both nutrients and
showed higher concentrations in the BAC+ experiments compared to the BAC- cultures (Fig. 2a,b).
Ammonium concentrations were consistently higher, and nitrate was removed more slowly in the

presence of bacteria, especially during the exponential phase. With the onset of the stationary phase in the BAC+ experiment, PO₄ and NH₄ concentrations doubled within 2 to 4 days and stayed high with
360 variations in phosphate concentrations, while they stayed low in BAC-. With depletion of NO₃ in BAC+,
NH₄ concentrations remained high, while PO₄ concentrations dropped. While not all ammonium
measured is also available for algae growth, discussion of the dynamics (decrease in the start, increase
with the onset of the stationary phase), especially if also shown in the EXT model, are still useful to
understand multi-nutrient dynamics (e.g. regeneration). Considering the overall higher concentrations of
365 NO₃, compared to NH₄, discussions of total DIN dynamics, DIN:DIP ratios, and limitations are also
meaningful. DOC values were very high from the start (approx. 2-4 mmol L⁻¹) and remained largely
constant throughout the experiment (Table A8).

The diatom *Chaetoceros socialis* grew exponentially in both treatments until day 8 before reaching a
stationary phase with declining cell numbers (Fig. 3). The growth rate of the BAC- culture (0.36 d⁻¹) was
370 slightly lower than in the treatment with bacteria present (0.42 d⁻¹) during the exponential phase. Algal
cellular abundance was higher in the BAC+ cultures. Towards the end of the exponential phase, the
diatom started to form noticeable aggregates in cultures with bacteria present, but only to a limited extent
in the BAC- cultures. Such aggregate formation with associated EPS production is typical for *C. socialis*.
With the onset of the stationary phase in the BAC+ cultures about 30% of the cells formed biofilms on
375 the walls of the cultivation bottles (estimated after sonication treatment). Bacteria (Fig. 3) continued to
grow throughout the entire experiment, but growth rates slowed down from 0.9 to 0.6 after day 8. In the
BAC- cultures, bacterial numbers increased after 8 days, but abundances remained two orders of
magnitude below the BAC+ cultures and effectively BAC- over the experimental incubation period. The
maximum photosynthetic quantum yield (Fv/Fm) is commonly used as a proxy of photosynthetic fitness
380 (high QY), indicating the efficiency of energy transfer after adsorption in photosystem II. Low values
are typically related to stress, including for example nitrogen (Cleveland and Perry, 1987), or silicate
(Lippemeier et al., 1999) limitation. We found an increase in QY from approx. 0.62 to 0.67 in the
exponential phase and a decrease to approx. 0.62 in the BAC+ treatment after 8 days and to approx. 0.58
in the BAC- treatment (Table A8).

385 During algal exponential growth, POC and PON concentrations followed changes in algal abundances
increasing four, seven, and 19-fold respectively, within 8 days (Fig. 3a, 4). Interestingly, with the
beginning of the stationary phase, POC and PON continued to increase in the BAC+ cultures, while their
concentrations stayed constant (POC), or decreased due to maintenance respiration (PON) in BAC-
cultures. POC and PON concentrations were consistently higher (1.2 times POC, 1.4 times PON) in
390 BAC+ cultures during the exponential phase. POC:PON ratios decreased in both cultures, but increased
again after 11 days in the BAC- culture. Chlorophyll *a* concentrations also increased exponentially over
the first eight days in both treatments, and thereafter decreased within the stationary phase in the BAC-
cultures. In contrast, cell numbers remained nearly constant in the BAC+ cultures, before declining at
the last sampling day.

395 Overall, both experimental cultures showed similar growth dynamics until day 8, with silicate becoming
limiting for both treatments and nitrogen only limiting in BAC- cultures. Algal growth with bacteria
present was slightly, but consistently higher during this phase. After eight days, algae growth stopped in
both treatments, but nitrogen and carbon were continuously assimilated in BAC+ cultures. BAC- cultures
started to degrade chlorophyll, while it stayed the same in BAC+ cultures. Algal abundances in the BAC+

400 treatment at the end of the experiment were ca 30% higher due to biofilm formation, and considerably
more carbon (2x total POC, or 10-20% per cell) and nitrogen (3x total PON) per cell had been assimilated,
and considerably more chlorophyll (2-3x total chlorophyll) produced at day 16. Cell size differences were
not detectable (ca 4 μ m diameter, Table A8). POC to PON ratios increased after 11 days in BAC- cultures
but showed no change in BAC+ cultures. POC to Chl ratios were comparable in both treatments (Fig. 5).
405 Assuming BAC- N fixation was mostly based on new production (nitrate as N source), while the algal N
fixation in bacterial enriched treatments was based on new and regenerated (ammonium as N source)
production, two-thirds of the production was based on regenerated production (f-ratio = 0.31).

3.2 Modelling

A comparison of the traditional G98 model with the EXT model allowed an estimate of importance of
410 bacterial DIN regeneration and Si co-limitations for describing the experimental growth dynamics. The
EXT model led to a slightly worse fit to the BAC- experiment ($RMSE_{G98} = 2.79$ $RMSE_{EXT} = 3.38$, Fig. 5
& 6). The real strength of the EXT model was in representing growth dynamics with bacteria present
(Fig. 5 & 6). Here, the RMSE was reduced by 47% from $RMSE_{G98} = 4.31$ down to $RMSE_{EXT} = 2.31$.
415 Both, the G98 and EXT model fits of the BAC- experiment were similarly good for POC and PON with
a slightly lower modelled growth rate. PON in the BAC+ experiment was poorly modelled without
consideration of silicate limitation or regenerated production specifically towards the end of the
exponential phase and during the stationary phase. Maximum PON values were about 3 times lower using
the G98 model (Fig. B3). In addition, the start of the stationary phase in the BAC+ experiment was
420 estimated 3 days too late via G98, even though modelled DIN was depleted three days too soon (Fig. B3).
Under BAC- conditions, where silicate limitation does not play a major role the G98 model appears
sufficient.

The EXT model allowed representing detailed dynamics in a bacteria influenced system such as the
responses to silicate limitation with a decrease in POC production, continued PON production, and the
stagnation of Chl synthesis (Fig. 5). Apart from the lag phase, the mass ratios of gC:gN and gC:gChl were
425 represented accurately (Fig. 5). The model fits of POC, PON and Chl without the separate carbon
excretion term (x_f) were lower compared to the model with excretion, indicating the importance of
excreted dissolved organic matter (DOM) concentrations ($RMSE_{EXT-exr}$ of 5.73).

DIN dynamics caused by ammonium – nitrate interactions were represented well (Fig. 6a). However, at
the onset of the stationary phase, ammonium concentrations of the model were one order of magnitude
430 lower than in the experiment, showing a major weakness (Fig. 6c). Increased weighting of ammonium
during the model fitting led to a slightly better fit to ammonium, but a substantially worse fit of the model
to POC, PON, and Chl ($RMSE_{EXT}=3.49$). This indicates that the problem lies with the ammonium data,
which include immobilized ammonium in the biofilm released during the filtration, but unavailable for
diatom growth. Other potential differences in biofilms were tested by means of different model extensions
435 (DOC and DON aggregation to EPS, increase DOM excretion). After including the DOC and DOM
aggregation to the model, the overall fit was improved ($RMSE_{EXT}=2.31$, $RMSE_{EXT+eps}=2.19$, Fig. S1).
However, in the absence of EPS data, we used the EXT model for the main discussion. Increased DOM
excretion could be explained by the SiPS term of the EXT model (Fig. S2). The silicate uptake estimation
was highly simplified using simple Monod kinetics, leading to too high modelled values in the stationary

440 phase and a too quick depletion in the start (Fig. 6d). Carbon excretion (x_f) lead to NO_x depletion after 8 days.

The sensitivity analysis (Table A4) revealed that the sensitivity of the added parameters in EXT is overall comparable to the sensitivity of the original parameters in G98. The model outputs were most sensitive to P_C^{Ref} ($L1=1.27$, $L2=2.05$), which is a parameter in both G98 and EXT. The most sensitive added
445 parameters in EXT were the DON excretion rate (x_f , $L1=0.17$, $L2=0.24$), the bacterial growth rate (μ_{bact} , $L1=0.18$, $L2=0.36$), and the remineralisation rate of refractory DON (rem_d , $L1=0.09$, $L2=0.21$), and the inhibition of photosynthesis under Si limitation (S_{IPS} , $L1=0.07$, $L2=0.18$), which was overall comparable to other sensitive parameters of the G98 model (Q_{max} , R^C , α_{Chl} , ζ , n , I , Θ_N^{max} , Table A1). Small
450 perturbations of the parameters only indirectly related to the fitted output variables did not lead to changes in POC, PON, Chl, or DIN.

4 Discussion

The experimental incubations showed that in the presence of bacteria both the growth period and gross carbon fixation were extended (Hypothesis I). The diatoms were able to continue photosynthesis under silicate limitation at a reduced rate as long as inorganic nitrogen was present (Hypothesis II). Overall, the
455 experimental incubations represented typical spring bloom dynamics for coastal Arctic systems, including an initial exponential growth phase terminated by N and Si limitation (Hypothesis III) and the potential for an extended growth period via regenerated production. Our model incorporating these results was able to reflect these dynamics by adding $\text{NH}_4\text{-NO}_3\text{-Si(OH)}_4$ co-limitations and bacterial NH_4 regeneration to the widely used G98 model. In addition, bacteria-algae interactions, DOC and biofilm dynamics were
460 important in the experiment, but those were not crucial for quantitatively modelling algal C:N:Chl quotas. While *C. socialis* may not be the dominant species in all coastal Arctic phytoplankton blooms, we argue that it is representative for chain-forming diatoms typically dominating these systems due to their shared needs and responses to nutrient limitations (e.g., Eilertsen et al., 1989; von Quillfeldt, 2005).

4.1 Silicon-nitrogen regeneration

465 Spring phytoplankton dynamics in Arctic and sub-Arctic coastal areas is typically characterized by an initial exponential growth of diatoms, followed by peaks of other taxa (like *Phaeocystis pouchetii*) soon after the onset of silicate limitation (Eilertsen et al. 1989). Thus, a shift in species composition for the secondary bloom is linked to silicate limitation prior to final bloom termination caused by inorganic nitrogen limitation. As suggested by our second hypothesis, photosynthesis was reduced by approx. 70%
470 after silicate became limiting, which is comparable to earlier experimental studies (Tezuka, 1989). However, as suggested by our first hypothesis, the secondary bloom was extended in time by bacterial regeneration of ammonium, allowing regenerated production to contribute about 69% of the total production ($f\text{-ratio}=0.31$) even during the diatom dominated scenario in our experimental incubation. With the start of the stationary phase, NH_4 and PO_4 concentrations doubled, presumably due to decreased
475 assimilation by the silicate-starved diatoms and increased regeneration by bacteria, supplied with increasing labile DOM (doubled remineralisation rate in EXT) excreted by the stressed algae. However, NH_4 concentrations doubled within four days, while PO_4 concentrations doubled in only one day,

indicating some unexplained internal dynamics, potentially via different bacterial uptake and release of N and P. After NO₃ depletion at day 15, also the PO₄ concentrations dropped, indicating a coupling of N:P metabolism, but not of NH₄:P metabolism. Thus, the sudden drop may also indicate dynamics of bottle experiments, not accounted for, showing potential limitations of these experiments. The presence of bacteria and thus regenerated production allowed diatom growth to continue 8 days after silicate became limiting (Figs. 2, 3 & 4), nearly doubling the growth period similar to observations in the field (e.g. Legendre and Rassoulzadegan, 1995; Johnson et al., 2007), which supports our Hypotheses I and III.

The G98 model has its most severe limitation in the modelling of PON, simply due to the lack of the ammonium pool, supplied via bacterial regeneration. The substantially better fit of PON in the EXT model shows therefore clearly that bacterial remineralisation is crucial to successfully model spring bloom dynamics, especially near bloom termination. Many biogeochemical models used in the Arctic include remineralisation but rely on fixed or temperature dependent rates and do not consider them bacteria-dependent (MEDUSA, LANL, NEMURO, NPZD, see Table 1). While this simplification allows modelling regenerated production, using bacteria-independent remineralisation rates does have limitations under spring bloom scenarios, where bacteria biomass can vary over orders of magnitudes (e.g. Sturluson et al., 2008) as also seen in our experimental study.

While we do not expect the f-ratio in our bottle experiment to be directly comparable to open ocean system due to the higher biodiversity of field communities, a comparison can aid to identify limitations in our experiment and model. The f-ratio can be used as a measure to check how representative the cultivation study was for typical spring bloom dynamics (Hypothesis III). Regenerated production is significant in polar systems and our estimated experimental f-value of 0.31 is slightly below the average for polar systems (Harrison and Cota, 1990, mean f-ratio=0.54). Nitrification is a process supplying about 50% of the NO₃ used for primary production in the oceans, which may lead to a substantial underestimation of regenerated production (Yool et al., 2007), inflating the f-ratio interpreted as estimate for new production, potentially also in the study by Harrison and Cota (1990). The absence of vertical PON export in our experiment may be another explanation for the above average fraction of regenerated production. In the ocean environment, regenerated production is also affected by vertical export (sedimentation) and grazing which are not represented in the experimental incubations. Via sedimentation, a fraction of the bloom either in the form of direct algal sinking or fecal pellets is typically exported to deeper water layers, reducing the potential for N regeneration within the euphotic zone (e.g. Keck and Wassmann, 1996). Larger zooplankton grazing can lead to increased export of PON via fecal pellet aggregation, or diel vertical migration (Banse, 1995), but may also release ammonium and urea (Conover and Gustavson, 1999, Saiz et al., 2013).

In contrast, bacterial death by microflagellate grazing and viral lysis may supply additional nutrients, or DON available for N regeneration in the euphotic zone (e.g. Goldman and Caron, 1985), which potentially leads to an overestimation of regenerated production. Another potentially important N source for regenerated production may be urea (Harrison et al., 1985), which would lead to an even higher importance of regenerated production as suggested by our study. Hence, ecosystem scale models will need to consider these dynamics regarding bacterial abundances, microbial networks and particle export in addition to bacterial remineralization in order to model realistic ammonium regeneration in the euphotic

520 zone. Overall, our cultivation experiment was powerful to represent major aspects of spring bloom
dynamics, but has its limitations, thereby confirming our third hypothesis only to some extent.
Bacteria-mediated silicate regeneration is absent from the modelling approach, as indicated by the
identical silicate concentrations in both treatments and models (Fig. 2d). In the environment silicate
dissolution is, in fact, mostly described as an abiotic process with temperature as the main control, and a
525 minor contribution by bacterial remineralisation (Bidle and Azam, 1999). Our experiment indicates that
silicate dissolution for *Chaetoceros socialis* was negligible at cold temperatures and the time scale of the
incubations and typical for bloom durations and residence times of algae cells in the euphotic zone
(Eilertsen et al., 1989, Keck and Wassmann, 1996). We conclude that silicate dissolution in coastal Arctic
systems happens most likely in the sediment or deeper water layers and is only supplied via mixing in
winter. In Antarctica substantial silicate dissolution has been observed but not in the upper 100 m, which
530 has been related to the low temperatures (Nelson and Gordon, 1981) in agreement with our conclusion.
Hence, modelling silicate regeneration in the euphotic zone is not necessary in these systems.

4.2 Algal growth response to Si and N limitation

The response of diatoms to Si or N limitation is based on different dynamics and different roles of N and
Si in diatom growth. N is needed for proteins and nucleic acids and its uptake is mainly driven by
535 phototrophic reactions (Martin-Jézéquel et al., 2000). Si is only needed for frustule formation and cell
division, mostly during a specific time in the cell cycle (G2 and M phase, Hildebrand, 2002) and the
assimilation is mostly driven by heterotrophic reactions (Martin-Jézéquel et al., 2000). Once N is limiting,
growth rapidly stops (Geider et al. 1998). In the case of Si limitation, however, growth can continue with
a slower rate if N is still available (Werner, 1978; Gilpin et al., 2004). Several studies found a reduced
540 growth rate with weaker silicified cell walls (Hildebrand, 2002; Gilpin, 2004), but unaffected nitrogen
assimilation under silicate limitation (Hildebrand 2002, Claquin et al., 2002) in accordance with our study.
Claquin et al. (2002) found variable Si:C and Si:N ratios and highly silicified cells under nitrogen
limitation, indicating uncoupled Si and N:C metabolism.

Nitrogen is a crucial element as part of amino acids and nucleic acids, which are necessary for cell activity
545 and growth. If N becomes limiting major cellular processes are affected and growth or chlorophyll
synthesis is not possible. Photosynthesis can continue for a while leading to carbon overconsumption
(Schartau et al., 2007), which is well modelled by G98 for both BAC+ and BAC-. A part of the excess
carbon can be stored as intracellular reserves, and a part is excreted as DOC, which may aggregate as
EPS, contributing to the total POC pool. The excess carbon can potentially be toxic for the algae and
550 excretion and extracellular degradation by bacteria may be crucial for algal survival (Christie-Oleza et
al., 2017). Quantitatively, N limitation is well modelled by G98 under BAC- conditions, if only one
nitrogen source plays a role. However, under longer nitrogen starvation times or higher light intensities,
alternative models that include carbon excretion and aggregation (Schartau et al., 2007) or intracellular
storage in reserve pools (Ross & Geider 2009) might be needed. Our growth experiment shows clearly,
555 that C:N ratios are not fixed and variable quotas are needed. Vichi et al. (2007) estimated that Carbon
based models that do not consider variable C/N ratios may underestimate net primary production (NPP)
by 50%, arguing for the importance of quota based models (Fransner et al., 2018). However, most
ecosystem scale models are simplified by using fixed C:N ratios (Table 1). The next step towards quota

560 based-models is the consideration of more detailed cell based characteristics, such as transporter density,
cell size, and mobility, including sedimentation (Aksnes and Egge, 1991). Flynn et al. (2018) discuss a
model with detailed uptake kinetics showing that large cells are overall disfavored over small cells due to
higher half saturation constants, but that they may still have competitive advantages due to lower
investment in transporter production. Also increased sedimentation in larger cells increases the mobility
and may offset the disadvantage of a larger size. While this extension is too complex for our aim of a
565 simplified model, the dynamics may become important when modelling different algae taxa.
The type of inorganic nitrogen available also affects nitrogen uptake. Due to the metabolic costs related
to intracellular nitrate reduction to ammonium, ammonium uptake is preferred over nitrate, potentially
leaving more energy for other processes (Lachmann et al., 2019). Ammonium can even inhibit or reduce
nitrate uptake over certain concentrations (Morris, 1974). The dynamics are mostly controlled by
570 intracellular processes, such as glutamate feedbacks on nitrogen assimilation, cost for nitrate conversion
to ammonium, or lower half saturation constants of ammonium transporters (Flynn et al., 1997). The most
accurate representation of these dynamics is given in the ANIM model by Flynn et al. (1997), but the
model is too complex for implementations in larger ecosystem models. The number of parameters is
difficult to tune with the typically limited availability of measured data and its complexity makes it also
575 computationally costly to scale up the models. Typically, modelling ammonium-nitrate interactions by
different half-saturation constants and inhibition of nitrate uptake by ammonium appears sufficient (e.g.,
BFM, LANL, NEMURO, Table 1) and has been adapted in our model.
Studies on the coupling of silicate limitation on C, N, and Chl show inconclusive patterns, including a
complete decoupling (Claquin et al., 2002), a relation of N to Si (Gilpin et al., 2004) and reduction of
580 photosynthesis without new chlorophyll production (Werner, 1978; Gilpin et al., 2004). Cell size is
limited by the frustules, but cells may become more nutritious (higher N:C ratio), or simply excrete more
DOM, which may aggregate and contribute to the PON and POC pools. A detailed cell-cycle based model
has been suggested by Flynn (2001), but the number of parameters (30) makes the model too complex for
ecosystem scale models. In ecosystem scale models Si limitation is modelled in various simplifications,
585 such as thresholds triggering a stop (MEDUSA), or reduction (e.g. BFM, MEDUSA, SINMOD) of the Si
dependent production (Table 1), or Si:N ratio scaled production (NEMURO, Table 1).
Our cultivation study shows i) that a threshold value in the model, leading to a stop or solely Si dependent
photosynthesis has its limitations, since DIN controlled photosynthesis continues at lower rates, and ii)
that coupling of Si:N:C:Chl is present. We do not expect a direct Si:N coupling, due to different controls
590 of Si and N metabolism (Martin-Jézéquel et al., 2000), but suggest indirect coupling via reduced
photosynthesis. In fact, detailed photophysiological and molecular approaches under Si limitation found
inhibited PSII reaction centers (Lippemeier et al., 1999) similar to the decreased QY in our experiment,
and down-regulated photosynthetic proteins (Thangaraj et al., 2019) under Si limitation. Thus, we
modelled the response of diatom growth to silicate limitation by reducing photosynthesis through a
595 parameterized fraction (S_{iPS}) and a stop of chlorophyll synthesis below a certain threshold, based on
experimental studies (Werner, 1978, Lippemeier et al., 1999, Gilpin et al., 2004, Thangaraj et al., 2019)
and in accordance to other ecosystem scale approaches. We suggest that this extension is more accurate
than the typical threshold-based dynamics, with one limiting nutrient controlling the growth equally for
POC and Chl production (e.g. SINMOD by Wassmann et al., 2006; BFM by Vichi et al., 2007), while

600 still keeping the number of parameters low compared to very detailed cell-cycle based models (e.g. Flynn, 2001, Flynn et al., 2018).

4.3 Importance of algae-bacteria interactions and DOC excretion

As described above, N or Si limitation can lead to excretion of DON and DOC, which can aggregate as EPS and be available for bacterial regeneration of ammonium. For accurately including EPS dynamics in the model additional data would be needed. However, the importance of EPS formation is evident in the end of the BAC+ experiment. Firstly, a biofilm was clearly visible containing about 30% of the algae cells. While we would not expect biofilms in the open ocean, aggregation of algae cells, facilitated by EPS is common towards the end of spring blooms, increasing vertical export fluxes (e.g. Thornton, 2002). *Chaetoceros socialis* is in fact a colony forming diatom building EPS-rich aggregates in nature (Booth et al., 2002). Secondly, POC and PON concentrations increased, while cell numbers and sizes stayed constant, showing that the additional POC and PON was most likely part of an extracellular pool. Silicate limitation could be one trigger for enhanced exudation. In fact, the biofilm dynamics evaluated (DOC aggregation, increased excretion) showed similar dynamics as the S_{EPS} term. Since the biofilm formation corresponds with silicate limitation, it is difficult to untangle the direct effects of the biofilm, or the indirect effects of silicate limitation, without additional data or experiments (e.g. EPS measurements, DOM characterization). However, our model run, including EPS aggregation allowed an improved overall fit, while reducing the S_{EPS} term to values more similar to earlier studies (Werner, 1978), pointing to the importance of DOC and DON aggregation. Hence, we suggest that Si limitation and EPS aggregation are both important.

620 Interestingly, algae – bacteria interactions can be species specific with specific organic molecules excreted by the algae to attract specific beneficial bacteria (Mühlenbruch et al., 2018). Thereby bacteria are crucial for recycling ammonium, but also to degrade potentially toxic exudates (Christie-Oleza et al., 2017).

In the BAC- experiment, Carbon excretion after Carbon overconsumption could be expected after Schartau et al. (2007), but no indications, such as biofilm formation, or increased POC per cell were found. In fact, a model considering EPS aggregation lead to a substantially worse fit to BAC-. This indicates that carbon overconsumption has been of minor importance likely due to the low light levels. An alternative explanation is that bacteria and potentially chemotaxis are important controls on algal carbon excretion (Mühlenbruch et al., 2018). Overall, DOM excretion and EPS dynamics appear to play a major role in quantitatively modelling C:N:Chl quotas in our experiment, with higher errors ($\text{RMSE}_{\text{EXT-exct}}=5.73$, $\text{RMSE}_{\text{EXT}}=2.31$) for a model run without than with the excretion term x_f .

4.4 Considerations in a changing climate

Due to a rapid changing climate, especially in Arctic coastal systems, the dynamics addressed in this study will change (Tremblay and Gagnon 2009). With warmer temperatures, heterotrophic activities, and thereby bacterial recycling will increase (Kirchman et al., 2009). Our study showed that regenerated production is crucial for an extended spring bloom. Hence, higher heterotrophic activities may lead to extended blooms (increased bacterial regeneration). At the same time, higher temperatures and increased

precipitation will lead to stronger and earlier stratified water columns, which will lead to less nutrients reaching the surface by winter mixing, reducing new production (decreased bacterial regeneration)(Tremblay and Gagnon, 2009; Fu et al., 2016). Consequently, the phenology of Arctic coastal primary production in a warmer climate will likely be increasingly driven by bacterial remineralization, showing the necessity to include this process into biogeochemical models. An earlier temperature driven water column stratification may also lead to an earlier bloom. However, due to increasing river and lake brownification and sediment resuspension, the spring bloom may also be delayed (Opdal et al., 2019). With decreased light, carbon overconsumption as described by Schartau et al. (2007) may become less important due to decreased photosynthesis. An earlier or later phytoplankton bloom can lead to a mismatch with zooplankton grazers (Durant et al., 2007; Sommer et al., 2007). Reduced zooplankton production would decrease the fecal pellet driven vertical export and thereby increase the residence time of POM in the euphotic zone and the potential for ammonium regeneration. Thus, the incorporation of bacterial recycling into ecosystem models may be even more important under this scenario. In fact, global climate change models agree that vertical carbon export is decreasing overall (Fu et al., 2016). Silicate regeneration is thought to be mostly controlled abiotically by temperature (Bidle and Azam, 1999). Thus, increasing temperature and a stronger stratification will allow recycling of silicate in the euphotic zone before sinking out and thus could cause a shift in the algal succession observed during spring with prolonged contributions of diatoms (Kamatani, 1982). Thus, a temperature dependent silica dissolution may need to be included for models in a substantially warmer climate in further model developments. Increased precipitation will also lead to increased runoff and allochthonous DOM inputs, increasing the importance of terrestrial DOM degradation and decreasing the relative importance of algal exudate regeneration (Jansson et al., 2008). The, low light levels, and the absence of grazing and export fluxes are simplifications of our study, which are, however, expected to be realistic scenarios under climate change. Hence, we suggest that our experiment and model are well suited as a baseline for predictive ecosystem models investigating the impacts of climate change on coastal Arctic spring blooms. However, climate change may lead to shifts in algae communities with non-silicifying algae dominating over diatoms (e.g. Falkowski and Oliver, 2007), reducing the importance of silicate limitation. Thus, conducting similar experiments and modelling exercises with a wider range of algal taxa and different temperature and nutrient regimes is suggested.

Acknowledgements

The project was supported by ArcticSIZE - A research group on the productive Marginal Ice Zone at UiT (project number 01vm/h15). We want to thank Paul Dubourg and Elzbieta Anna Petelenz-Kurdziel for the help with Nutrient and POC/PON analyses. DOC analyses were supported through a Fulbright Distinguished Scholar Award to HRH.

Authors contributions

TRV designed the experiment with contributions by RG and ML. TRV isolated and identified the cultures. ML performed the experiment with contributions of TRV and UD. RH measured DOC and SK measured

675 the Nutrients. The other parameters were measured by ML and TRV. TRV programmed the model with contributions of CV, ST and DvO. TRV wrote the manuscript with contributions from all co-authors.

Data availability

The experimental data are archived at DataverseNO under the doi number doi.org/10.18710/VA4IU9. The Rscripts for the model used in this publication are archived at zenodo
680 (doi.org/10.5281/zenodo.4459550) and available at github under
https://github.com/tvonnahm/Dynamic-Algae-Bacteria-model.

Competing interests

The authors declare that they have no conflict of interest.

References

- 685 Al Khudary, R., Stößer, N. I., Qoura, F., and Antranikian, G.: *Pseudoalteromonas arctica* sp. nov., an aerobic, psychrotolerant, marine bacterium isolated from Spitzbergen, Int. J. Syst. Evol. Microbiol., 58, 2018-2024, 2008.
- Alcaraz, M., Almeda, R., Calbet, A., Saiz, E., Duarte, C. M., Lasternas, S., Agusti, S., Santiago, R., Movilla, J., and Alonso, A.: The role of arctic zooplankton in biogeochemical cycles: respiration and
690 excretion of ammonia and phosphate during summer, Polar Biol., 33(12), 1719-1731, 2010.
- Altschul, S. F., Gish, W., Miller, W., Myers, E. W. and Lipman, D. J.: Basic local alignment search tool, J. Mol. Biol., 215, 403-410, 1990.
- Alver, M. O., Broch, O. J., Melle, W., Bagøien, E., and Slagstad, D.: Validation of an Eulerian population model for the marine copepod *Calanus finmarchicus* in the Norwegian Sea, J Mar Syst, 160, 81-93, 2016.
- 695 Aksnes, D. L., and Egge, J. K.: A theoretical model for nutrient uptake in phytoplankton, Mar. Ecol. Prog. Ser., 70(1), 65-72, 1991.
- Amin, S. A., Parker, M. S., and Armbrust, E. V.: Interactions between diatoms and bacteria, Microbiol. Mol. Biol. Rev., 76(3), 667-684, 2012.
- Amin, S. A., Hmelo, L. R., Van Tol, H. M., Durham, B. P., Carlson, L. T., Heal, K. R., Morales, R. L.,
700 Berthiaume, C. T., Parker, M. S., Djunaedi, B., Ingalls, A. E., Parsek, M. R., Moran, M. A., and Armbrust, E. V.: Interaction and signalling between a cosmopolitan phytoplankton and associated bacteria, Nature, 522, 98-101, 2015.
- Andersen, R. A., and Kawachi, M.: Microalgae isolation techniques, in: Algal culturing techniques, edited by: Andersen, R. A., Elsevier, 83, 2005.
- 705 Anju, M., Sreesh, M. G., Valsala, V., Smitha, B. R., Hamza, F., Bharathi, G., and Naidu, C. V.: Understanding the role of nutrient limitation on plankton biomass over Arabian Sea via 1-D coupled biogeochemical model and Bio-Argo observations, J. Geophys. Res. Oceans, 125(6), 2020.

- Banse, K.: Zooplankton: pivotal role in the control of ocean production: I. Biomass and production, ICES J. Mar. Sci., 52, 265-277, 1995.
- 710 Bertani, G.: Lysogeny at mid-twentieth century: P1, P2, and other experimental systems, J. Bacteriol., 186, 595-600, 2004.
- Bidle, K. D., and Azam, F.: Accelerated dissolution of diatom silica by marine bacterial assemblages, Nature, 397, 508-512, 1999.
- Booth, B. C., Larouche, P., Bélanger, S., Klein, B., Amiel, D., and Mei, Z. P.: Dynamics of *Chaetoceros socialis* blooms in the North Water, Deep Sea Res. Part II Top. Stud. Oceanogr., 49, 5003-5025, 2002.
- 715 Brun, R., Reichert, P. and Kunsch, H. R.: Practical identifiability analysis of large environmental simulation models, Water Resour. Res. 37(4): 1015–1030, 2001.
- Burdige, D.J., and Homstead, J.: Fluxes of dissolved organic carbon from Chesapeake Bay sediments. Geochim. Cosmochim. Acta, 58, 3407-3424, 1994.
- 720 Christie-Oleza, J. A., Sousoni, D., Lloyd, M., Armengaud, J., and Scanlan, D. J.: Nutrient recycling facilitates long-term stability of marine microbial phototroph–heterotroph interactions, Nat Microbiol, 2, 17100, 2017.
- Claquin, P., Martin-Jézéquel, V., Kromkamp, J. C., Veldhuis, M. J. W., and Kraay, G. W.: Uncoupling of silicon compared with carbon and nitrogen metabolisms and the role of the cell cycle in continuous
- 725 cultures of *Thalassiosira pseudonana* (Bacillariophyceae) under light, nitrogen, and phosphorus control, J. Phycol., 38(5), 922–930, 2002.
- Cleveland, J. S., & Perry, M. J.: Quantum yield, relative specific absorption and fluorescence in nitrogen-limited *Chaetoceros gracilis*. Marine Biology, 94(4), 489-497, 1987.
- Conover, R. J., and Gustavson, K. R.: Sources of urea in arctic seas: zooplankton metabolism, Mar. Ecol. Prog. Ser., 179, 41-54, 1999.
- 730 Degerlund, M., and Eilertsen, H. C.: Main species characteristics of phytoplankton spring blooms in NE Atlantic and Arctic waters (68–80 N), Estuar. Coast, 33, 242-269, 2010.
- Dortch, Q.: The interaction between ammonium and nitrate uptake in phytoplankton. Mar. Ecol. Prog. Ser., Oldendorf, 61, 183-201, 1990.
- 735 Durant, J. M., Hjermann, D. Ø., Ottersen, G., and Stenseth, N. C.: Climate and the match or mismatch between predator requirements and resource availability, Clim. Res., 33, 271-283, 2007.
- Egge, J. K., and Aksnes, D.L.: Silicate as regulating nutrient in phytoplankton competition, Mar. Ecol. Prog. ser., 83, 281-289, 1992.
- Eilertsen, H. C., and Frantzen, S.: Phytoplankton from two sub-Arctic fjords in northern Norway 2002–
- 740 2004: I. Seasonal variations in chlorophyll a and bloom dynamics, Mar. Biol. Res., 3, 319-332, 2007.
- Eilertsen, H. C., Taasen, J. P., and Weslawski, J. M.: Phytoplankton studies in the fjords of West Spitzbergen: physical environment and production in spring and summer, J. Plankton Res., 11, 1245-1260, 1989.
- Eppley, R. W., Rogers, J. N., and McCarthy, J. J.: Half-saturation constants for uptake of nitrate and ammonium by marine phytoplankton, Limnol. Oceanogr., 14(6), 912-920, 1969.
- 745 Eppley, R. W.: Autotrophic production of particulate matter, Analysis of marine ecosystems/AR Longhurst, 1981.
- Falkowski, P. G., and Oliver, M. J.: Mix and match: how climate selects phytoplankton, Nat. Rev. Microbiol., 5, 813-819, 2007.

- 750 Field, C. B., Behrenfeld, M. J., Randerson, J. T., and Falkowski, P.: Primary production of the biosphere: integrating terrestrial and oceanic components, *Science*, 281, 237-240, 1998.
- Firme, G. F., Rue, E. L., Weeks, D. A., Bruland, K. W., and Hutchins, D. A.: Spatial and temporal variability in phytoplankton iron limitation along the California coast and consequences for Si, N, and C biogeochemistry, *Global Biogeochem Cycles*, 17(1), 2003.
- 755 Flynn, K. J.: A mechanistic model for describing dynamic multi-nutrient, light, temperature interactions in phytoplankton, *J. Plankton Res.*, 23, 977-997, 2001.
- Flynn, K. J.: Modelling multi-nutrient interactions in phytoplankton; balancing simplicity and realism, *Prog. Oceanogr.*, 56, 249-279, 2003.
- Flynn, K. J., and Fasham, M. J.: A short version of the ammonium-nitrate interaction model, *J. Plankton Res.*, 19, 1881-1897, 1997.
- 760 Flynn, K. J., Fasham, M. J., and Hipkin, C. R.: Modelling the interactions between ammonium and nitrate uptake in marine phytoplankton. *PHILOS T R SOC A, Series B: Biological Sciences*, 352, 1625-1645, 1997.
- Flynn, K. J.: Nitrate transport and ammonium-nitrate interactions at high nitrate concentrations and low temperature, *Mar. Ecol. Prog. Ser.*, 187, 283-287, 1999.
- 765 Flynn, K. J., Marshall, H., and Geider, R. J.: A comparison of two N-irradiance interaction models of phytoplankton growth, *Limnol. Oceanogr.*, 46, 1794-1802, 2001.
- Flynn, K. J., Skibinski, D. O., and Lindemann, C.: Effects of growth rate, cell size, motion, and elemental stoichiometry on nutrient transport kinetics, *PLoS Comput. biology*, 14(4), 2018.
- 770 Fransner, F., Gustafsson, E., Tedesco, L., Vichi, M., Hordoir, R., Roquet, F., Spilling, K., Kuznetsov, I., Eilola, K., Mörth, C., Humborg, C., and Nycander, J.: Non-Redfieldian dynamics explain seasonal pCO₂ drawdown in the Gulf of Bothnia, *J Geophys Res Oceans*, 123, 166-188, 2017.
- Fritz, M., Vonk, J. E., and Lantuit, H.: Collapsing arctic coastlines, *Nat Clim Chang*, 7, 6, 2017.
- Fu, W., Randerson, J. T., and Moore, J. K.: Climate change impacts on net primary production (NPP) and export production (EP) regulated by increasing stratification and phytoplankton community structure in the CMIP5 models, *Biogeosciences*, 13, 5151-5170, 2016.
- 775 Geider, R., and La Roche, J.: Redfield revisited: variability of C: N: P in marine microalgae and its biochemical basis, *European J. Phycol.*, 37(1), 1-17, 2002.
- Geider, R. J., MacIntyre, H. L., and Kana, T. M.: A dynamic regulatory model of phytoplanktonic acclimation to light, nutrients, and temperature, *Limnol. Oceanogr.*, 43, 679-694, 1998.
- 780 Gilpin, L.: The influence of changes in nitrogen: silicon ratios on diatom growth dynamics, *J. Sea Res.*, 51, 21-35, 2004.
- Goldman, J. C., and Caron, D. A.: Experimental studies on an omnivorous microflagellate: implications for grazing and nutrient regeneration in the marine microbial food chain, *Deep Sea Res A*, 32, 899-915, 1985.
- 785 Gruber, N., Frenzel, H., Doney, S. C., Marchesiello, P., McWilliams, J. C., Moisan, J. R., Oram, J. J., Plattner, G., and Stolzenbach, K. D.: Eddy-resolving simulation of plankton ecosystem dynamics in the California Current System, *Deep Sea Res. Part I Oceanogr. Res. Pap.*, 53(9), 1483-1516, 2006.
- Guillard, R. L. L.: Culture of phytoplankton for feeding marine invertebrates, in: *Culture of marine invertebrates animals*, edited by: Smith, W. L., Chanley, M. H., Plenum Press, New York, 29-60, 1975.
- 790

- Harrison, W. G., Head, E. J. H., Conover, R. J., Longhurst, A. R., and Sameoto, D. D.: The distribution and metabolism of urea in the eastern Canadian Arctic, *Deep Sea Res. Part I Oceanogr. Res.*, 32(1), 23-42 1985.
- 795 Harrison, W. G., and Cota, G. F.: Primary production in polar waters: relation to nutrient availability, *Polar Res*, 10, 87-104, 1991
- Haecky, P., & Andersson, A.: Primary and bacterial production in sea ice in the northern Baltic Sea, *Aquat. Microb. Ecol.*, 20(2), 107-118, 1999.
- Hauck, J., Völker, C., Wang, T., Hoppema, M., Losch, M., & Wolf-Gladrow, D. A.: Seasonally different carbon flux changes in the Southern Ocean in response to the southern annular mode, *Global Biogeochem Cycles*, 27, 1–10, 2013.
- 800 Henson, S. A., Cole, H. S., Hopkins, J., Martin, A. P., and Yool, A.: Detection of climate change-driven trends in phytoplankton phenology, *Glob. Change Biol.*, 24(1), e101-e111, 2018.
- Hildebrand, M.: Lack of coupling between silicon and other elemental metabolisms in diatoms, *J. Phycol.*, 38, 841–843, 2002.
- 805 Hohn, S.: A model of the carbon:nitrogen:silicon stoichiometry of diatoms based on metabolic processes, PhD thesis, Universität Bremen, Bremen, 43-57, 2009.
- Hünken, M., Harder, J., and Kirst, G. O.: Epiphytic bacteria on the Antarctic ice diatom *Amphiprora kufferathii* Manguin cleave hydrogen peroxide produced during algal photosynthesis, *Plant Biol.*, 10, 519-526, 2008.
- 810 Iversen, K. R., and Seuthe, L.: Seasonal microbial processes in a high-latitude fjord (Kongsfjorden, Svalbard): I. Heterotrophic bacteria, picoplankton and nanoflagellates, *Polar Biol.*, 34, 731-749, 2011.
- Jacobsen, T. R., and Rai, H.: Comparison of spectrophotometric, fluorometric and high performance liquid chromatography methods for determination of chlorophyll a in aquatic samples: effects of solvent and extraction procedures, *Internationale Revue der gesamten Hydrobiologie und Hydrographie*, 75, 207-217, 1990.
- 815 Jansson, M., Hickler, T., Jonsson, A. and Karlsson, J.: Links between terrestrial primary production and bacterial production and respiration in lakes in a climate gradient in subarctic Sweden, *Ecosystems*, 11, 367–376, 2008.
- Johnson, M., Sanders, R., Avgoustidi, V., Lucas, M., Brown, L., Hansell, D., Moore, M., Gibb, S., Liss, P., and Jickells, T.: Ammonium accumulation during a silicate-limited diatom bloom indicates the potential for ammonia emission events, *Mar Chem*, 106, 63-75, 2007.
- 820 Kamatani, A.: Dissolution rates of silica from diatoms decomposing at various temperatures, *Mar. Biol.*, 68, 91– 96, 1982.
- Keck, A., and Wassmann, P.: Temporal and spatial patterns of sedimentation in the subarctic fjord Malangen, northern Norway, *Sarsia*, 80, 259-276, 1996.
- 825 Kim, S. J., Kim, B. G., Park, H. J., and Yim, J. H.: Cryoprotective properties and preliminary characterization of exopolysaccharide (P-Arcpo 15) produced by the Arctic bacterium *Pseudoalteromonas elyakovii* Arcpo 15, *Prep. Biochem. Biotechnol.*, 46, 261-266, 2016.
- Kirchman, D. L.: Uptake and regeneration of inorganic nutrients by marine heterotrophic bacteria, *Microbial ecology of the oceans*, 2000.
- 830 Kirchman, D. L., Morán, X. A. G., and Ducklow, H.: Microbial growth in the polar oceans—role of temperature and potential impact of climate change, *Nat. Rev. Microbiol.*, 7, 451-459, 2009.

- Kishi, M. J., Kashiwai, M., Ware, D. M., Megrey, B. A., Eslinger, D. L., Werner, F. E., Noguchi-Aita, M., Azumaya, T., Fujii, M., Hashimoto, S., Huang, D., Iizumi, H., Ishida, Y., Kang, S., Kantakov, G. A.,
835 Kim, H., Komatsu, K., Navrotsky, V. V., Smith, S. L., Tadokoro, K., Tsuda, A., Yamamura, O.,
Yamanaka, Y., Yokouchi, K., Yoshie, N., Zhang, J., Zuenko, Y. I., and Zvalinsky, V. I.: NEMURO – a
lower trophic level model for the North Pacific marine ecosystem, *Ecol. Model.*, 202, 12–25, 2007.
- Krause, J. W., Schulz, I. K., Rowe, K. A., Dobbins, W., Winding, M. H., Sejr, M. K., Duarte, C. M., and
840 Agustí, S.: Silicic acid limitation drives bloom termination and potential carbon sequestration in an Arctic
bloom, *Sci Rep*, 9(1), 1-11, 2019.
- Lachmann, S. C., Mettler-Altmann, T., Wacker, A., & Spijkerman, E.: Nitrate or ammonium: Influences
of nitrogen source on the physiology of a green algae, *Ecol. Evol.*, 9(3), 1070-1082, 2019.
- Lannuzel, D., Tedesco, L., Van Leeuwe, M., Campbell, K., Flores, H., Delille, B., Miller, L., Stefels, J.,
Assmy, P., Bowman, J., Brown, K., Castellani, G., Chierici, M., Crabeck, O., Damm, E., Else, B.,
845 Fransson, A., Fripiat, F., Geilfus, N., Jacques, C., Jones, E., Kaartokallio, H., Kotovitch, M., Meiners, K.,
Moreau, S., Nomura, D., Peeken, I., Rintala, J., Steiner, N., Tison, J., Vancoppenolle, M., van der Linden,
F., Vichi, M., and Wongpan, P.: The future of Arctic sea-ice biogeochemistry and ice-associated
ecosystems, *Nat. Clim. Change*, 1-10, 2020.
- Le Quéré, C., Andrew, R. M., Canadell, J. G., Sitch, S., Korsbakken, J. I., Peters, G. P., Manning, A. C.,
850 Boden, T. A., Tans, P. P., Houghton, R. A., Keeling, R. F., Alin, S., Andrews, O. D., Anthoni, P., Barbero,
L., Bopp, L., Chevallier, F., Chini, L. P., Ciais, P., Currie, K., Delire, C., Doney, S. C., Friedlingstein, P.,
Gkritzalis, T., Harris, I., Hauck, J., Haverd, V., Hoppema, M., Klein Goldewijk, K., Jain, A. K., Kato, E.,
Körtzinger, A., Landschützer, P., Lefèvre, N., Lenton, A., Lienert, S., Lombardozzi, D., Melton, J. R.,
855 Metzl, N., Millero, F., Monteiro, P. M. S., Munro, D. R., Nabel, J. E. M. S., Nakaoka, S.-I., O'Brien, K.,
Olsen, A., Omar, A. M., Ono, T., Pierrot, D., Poulter, B., Rödenbeck, C., Salisbry, J., Schuster, U.,
Schwinger, J., Séférian, R., Skjelvan, I., Stocker, B. D., Sutton, A. J., Takahashi, T., Tian, H., Tilbrook,
B., van der Laan-Luijkx, I. T., van der Werf, G. R., Viovy, N., Walker, A. P., Wiltshire, A. J., and Zaehle,
S.: Global carbon budget 2016, *Earth Syst Sci Data*, 8(2), 605-649, 2016.
- Lee, S., and Fuhrman, J. A.: Relationships between biovolume and biomass of naturally derived marine
860 bacterioplankton, *Appl. Environ. Microbiol.*, 53(6), 1298-1303, 1987.
- Legendre, L., and Rassoulzadegan, F.: Plankton and nutrient dynamics in marine waters, *Ophelia*, 41,
153-172, 1995
- Lippemeier, S., Hartig, P., and Colijn, F.: Direct impact of silicate on the photosynthetic performance of
the diatom *Thalassiosira weissflogii* assessed by on-and off-line PAM fluorescence measurements, *J.*
865 *Plankton Res.*, 21(2), 1999.
- Loebl, M., Colijn, F., van Beusekom, J. E., Baretta-Bekker, J. G., Lancelot, C., Philippart, C. J., Rousseau,
V., and Wiltshire, K. H.: Recent patterns in potential phytoplankton limitation along the Northwest
European continental coast, *J. Sea Res.*, 61, 34-43, 2009.
- Ma, L. Y., Chi, Z. M., Li, J., and Wu, L. F.: Overexpression of alginate lyase of *Pseudoalteromonas*
870 *elyakovii* in *Escherichia coli*, purification, and characterization of the recombinant alginate lyase, *World*
J. Microbiol. Biotechnol., 24, 89-96, 2008.
- Martin-Jézéquel, V., Hildebrand, M., and Brzezinski, M. A.: Silicon Metabolism in Diatoms: Implications
for Growth, *J. Phycol.*, 36, 821–840, 2000.

- Mills, M. M., Brown, Z. W., Laney, S. R., Ortega-Retuerta, E., Lowry, K. E., Van Dijken, G. L., and
875 Arrigo, K. R.: Nitrogen limitation of the summer phytoplankton and heterotrophic prokaryote
communities in the Chukchi Sea, *Front. Mar. Sci.*, 5, 362, 2018.
- Moore, J. K., Doney, S. C., and Lindsay, K.: Upper ocean ecosystem dynamics and iron cycling in a
global three-dimensional model, *Global Biogeochem Cycles*, 18, 2004.
- Moore, C. M., Mills, M. M., Arrigo, K. R., Berman-Frank, I., Bopp, L., Boyd, P. W., Galbraith, E. D.,
880 Geider, R. J., Guieu, C., Jac-card, S. L., Jickells, T. D., La Roche, J., Lenton, T. M., Ma-howald,
N. M., Maranon, E., Marinov, I., Moore, J. K., Nakat-suka, T., Oschlies, A., Saito, M. A., Thingstad, T.
F., Tsuda, A., and Ulloa, O.: Processes and patterns of oceanic nutrient limitation, *Nat Geosci*, 6, 701-710,
2013.
- Morris, I.: Nitrogen assimilation and protein synthesis, *Algal physiology and biochemistry*, 10, 1974.
- 885 Mühlenbruch, M., Grossart, H. P., Eigemann, F., and Voss, M.: Mini-review: Phytoplankton-derived
polysaccharides in the marine environment and their interactions with heterotrophic bacteria, *Environ.
Microbiol.*, 20, 2671-2685, 2018.
- Nelson, D. M., & Gordon, L. I.: Production and pelagic dissolution of biogenic silica in the Southern
Ocean, *Geochim. Cosmochim. Acta*, 46(4), 491-501, 1982.
- 890 Nelson, D. M., Treguer, P., Brzezinski, M. A., Leynaert, A., and Queguiner, B.: Production and
dissolution of biogenic silica in the ocean: revised global estimates, comparison with regional data and
relationship to biogenic sedimentation, *Glob. Biogeochem. Cycles*, 9, 359–372, 1995.
- Opdal, A. F., Lindemann, C., and Aksnes, D. L.: Centennial decline in North Sea water clarity causes
strong delay in phytoplankton bloom timing, *Glob. Change Biol.*, 25(11), 3946-3953, 2019.
- 895 Pahlow, M.: Linking chlorophyll-nutrient dynamics to the Redfield N: C ratio with a model of optimal
phytoplankton growth, *Mar. Ecol. Prog. Ser.*, 287, 33-43, 2005.
- Pedersen, M. F., and Borum, J.: Nutrient control of algal growth in estuarine waters. Nutrient limitation
and the importance of nitrogen requirements and nitrogen storage among phytoplankton and species of
macroalgae, *Mar. Ecol. Prog. Ser.*, 142, 261-272, 1996
- 900 Pella E, Colombo B. Study of carbon, hydrogen and nitrogen determination by combustion-gas
chromatography, *Microchim Acta*. 61, 697–719, 1973.
- Ratkova, T. N., Wassmann, P.: Seasonal variation and spatial distribution of phyto- and protozooplankton
in the central Barents Sea, *J Mar Syst*, 38, 47-75, 2002.
- Redfield, A. C.: On the proportions of organic derivatives in sea water and their relation to the
905 composition of plankton, James Johnstone memorial volume, 176-192, 1934.
- Rey, F., Skjoldal, H. R.: Consumption of silicic acid below the euphotic zone by sedimenting diatom
blooms in the Barents Sea, *MEPS*, 36, 307-312, 1987.
- Ross, O. N., and Geider, R. J.: New cell-based model of photosynthesis and photo-acclimation:
accumulation and mobilisation of energy reserves in phytoplankton, *Mar. Ecol. Prog. Ser.*, 383, 53-71,
910 2009.
- Saiz, E., Calbet, A., Isari, S., Anto, M., Velasco, E. M., Almeda, R., Movilla, J., and Alcaraz, M.:
Zooplankton distribution and feeding in the Arctic Ocean during a *Phaeocystis pouchetii* bloom, *Deep
Sea Res. Part I Oceanogr. Res. Pap.*, 72, 17-33, 2013.

- Schartau, M., Engel, A., Schröter, J., Thoms, S., Völker, C., and Wolf-Gladrow, D.: Modelling carbon overconsumption and the formation of extracellular particulate organic carbon, *Biogeosciences*, 4, 13-67, 2007.
- Schourup-Kristensen, V., Wekerle, C., Wolf-Gladrow, D., and Völker, C.: Arctic Ocean biogeochemistry in the high resolution FESOM 1.4-REcoM2 model, *Prog. Oceanogr.*, 168, 65-81, doi:10.1016/j.pocean.2018.09.006, 2018.
- Slagstad, D., Wassmann, P. F., and Ellingsen, I.: Physical constrains and productivity in the future Arctic Ocean, *Front Mar Sci*, 2, 85, 2015.
- Smith, K. M., Kern, S., Hamlington, P. E., Zavatarelli, M., Pinardi, N., Klee, E. F., and Niemeyer, K. E.: BFM17 v1. 0: Reduced-Order biogeochemical flux model for upper ocean biophysical simulations, *Geoscientific Model Development Discussions*, 1-35, 2020.
- Soetaert, K. and Herman, P. M. J.: *A Practical Guide to Ecological Modelling -- Using R as a Simulation Platform*, Springer, 390 pp, 2009.
- Soetaert, K., Petzoldt, T.: Inverse Modelling, Sensitivity and Monte Carlo Analysis in R Using Package FME, *J Stat Softw*, 33, 1–28, doi: 10.18637/jss.v033.i03, 2010.
- Soetaert, K., Petzoldt, T., and Setzer, R. W.: Solving Differential Equations in R: Package deSolve, *J Stat Softw*, 33, 1548-7660, doi: 10.18637/jss.v033.i09, 2010.
- Sommer, U., Aberle, N., Engel, A., Hansen, T., Lengfellner, K., Sandow, M., Wohlers, J., Zollner, E., and Riebesell, U.: An indoor mesocosm system to study the effect of climate change on the late winter and spring succession of Baltic Sea phyto-and zooplankton, *Oecologia*, 150, 655-667, 2007.
- Spilling, K., Tamminen, T., Andersen, T., and Kremp, A.: Nutrient kinetics modeled from time series of substrate depletion and growth: dissolved silicate uptake of Baltic Sea spring diatoms, *Mar. Biol.*, 157, 427-436, 2010
- Stow, C. A., Jolliff, J., McGillicuddy Jr, D. J., Doney, S. C., Allen, J. I., Friedrichs, M. A., Kenneth, A. R., and Wallhead, P.: Skill assessment for coupled biological/physical models of marine systems, *J Mar Syst*, 76, 4-15, 2009.
- Sturluson, M., Nielsen, T. G., and Wassmann, P.: Bacterial abundance, biomass and production during spring blooms in the northern Barents Sea, *Deep Sea Res. Part II Top. Stud. Oceanogr.*, 55, 2186-2198, 2008.
- Sverdrup, H. U.: On conditions for the vernal blooming of phytoplankton, *Cons. Perm. Int. Expl. Mer*, 18, 287-295, 1953.
- Teeling, H., Fuchs, B. M., Becher, D., Klockow, C., Gardebrecht, A., Bennke, C. M., Kassabgy, M., Huang, S., Mann, A. J., Waldmann, J., Weber, M., Klindworth, A., Otto, A., Lange, J., Bernhardt, J., Reinsch, C., Hecker, M., Peplies, J., Bockelmann, F. D., Callies, U., Gerds, G., Wichels, A., Wiltshire, K. H., Glöckner, F. O., Schweder, T., and Amann, R.: Substrate-controlled succession of marine bacterioplankton populations induced by a phytoplankton bloom, *Science*, 336, 608-611, 2012.
- Teeling, H., Fuchs, B. M., Bennke, C. M., Krueger, K., Chafee, M., Kappelmann, L., Reintjes, G., Waldmann, J., Quast, C., Glöckner, F. O., Lucas, J., Wichels, A., Gerds, G., Wiltshire, K. H., Amann, R.: Recurring patterns in bacterioplankton dynamics during coastal spring algae blooms, *Elife*, 5, 2016.
- Tezuka, Y.: The C: N: P ratio of phytoplankton determines the relative amounts of dissolved inorganic nitrogen and phosphorus released during aerobic decomposition, *Hydrobiologia*, 173, 55-62, 1989.

- 955 Thangaraj, S., Shang, X., Sun, J., and Liu, H.: Quantitative proteomic analysis reveals novel insights into intracellular silicate stress-responsive mechanisms in the diatom *Skeletonema dohrnii*, *Int. J. Mol. Sci.*, 20(10), 2540, 2019.
- Thornton, D.: Diatom aggregation in the sea: mechanisms and ecological implications, *Eur. J. Phycol.*, 37(2), 149-161, 2002.
- 960 Tremblay, J. É., and Gagnon, J.: The effects of irradiance and nutrient supply on the productivity of Arctic waters: a perspective on climate change, in: *Influence of climate change on the changing arctic and sub-arctic conditions*, edited by: Nihoul, J. C., J., Kostianoy, A. G., Springer, Dordrecht, 73-93, 2009.
- Uitz, J., Claustre, H., Gentili, B., and Stramski, D.: Phytoplankton class-specific primary production in the world's oceans: Seasonal and interannual variability from satellite observations, *Global Biogeochem Cycles*, 24, 2010.
- 965 Van den Meersche, K., Middelburg, J. J., Soetaert, K., Van Rijswijk, P., Boschker, H. T., and Heip, C. H.: Carbon-nitrogen coupling and algal-bacterial interactions during an experimental bloom: Modeling a ¹³C tracer experiment, *Limnol. Oceanogr.*, 49, 862-878, 2004.
- Vichi, M., Pinardi, N., and Masina, S.: A generalized model of pelagic biogeochemistry for the global ocean ecosystem. Part I: Theory, *J Mar Syst*, 64, 89-109, 2007.
- 970 von Quillfeldt, C. H.: Common diatom species in Arctic spring blooms: Their distribution and abundance, *Botanica Marina*, 43(6), 499-516, <https://doi.org/10.1515/BOT.2000.050>, 2005.
- Wassmann, P., Slagstad, D., Riser, C. W., and Reigstad, M.: Modelling the ecosystem dynamics of the Barents Sea including the marginal ice zone: II. Carbon flux and interannual variability, *J Mar Syst*, 59, 975 1-24, 2006.
- Weitz, J. S., Stock, C. A., Wilhelm, S. W., Bourouiba, L., Coleman, M. L., Buchan, A., Follows, M.J., Fuhrman, J. A., Jover, L., Lennon, J. T., Middelboe, M., Sonderegger, D. L., Suttle, C. A., Taylor, B. P., Thingstad, T. F., Wilson, W., and Wommack, K. E.: A multitrophic model to quantify the effects of marine viruses on microbial food webs and ecosystem processes, *ISME J*, 9, 1352-1364, 2015.
- 980 Werner, D.: Silicate metabolism, in: *The biology of diatoms*, edited by: Werner, D., Blackwell Scientific Publications, California, 13, 111-149, 1977.
- Werner, D.: Regulation of metabolism by silicate in diatoms, in: *Biochemistry of silicon and related problems*, edited by: Bendz, G., and Lindqvist, I., Springer, Boston, MA, 149-176, 1978.
- Westberry, T. K., Behrenfeld, M. J., Siegel, D. A., Boss, E.: Carbon-based primary productivity modeling with vertically resolved photoacclimation, *Global Biogeochem Cycles*, 22, 1-18, 2008.
- 985 Wu, Y., Liu, S., Huang, Z., and Yan, W.: Parameter optimization, sensitivity, and uncertainty analysis of an ecosystem model at a forest flux tower site in the United States, *J. adv. model. earth syst.*, 6(2), 405-419, 2014.
- Yool, A., Martin, A. P., Fernández, C., and Clark, D. R.: The significance of nitrification for oceanic new production, *Nature*, 447(7147), 999-1002, 2007.
- 990 Yool, A., and Popova, E. E.: Medusa-1.0: a new intermediate complexity plankton ecosystem model for the global domain, *Geosci Model Dev*, 4, 381, 2011.
- Zambrano, J., Krustok, I., Nehrenheim, E., and Carlsson, B.: A simple model for algae-bacteria interaction in photo-bioreactors, *Algal Res*, 19, 155-161, 2016.
- 995

1000 **Figures**

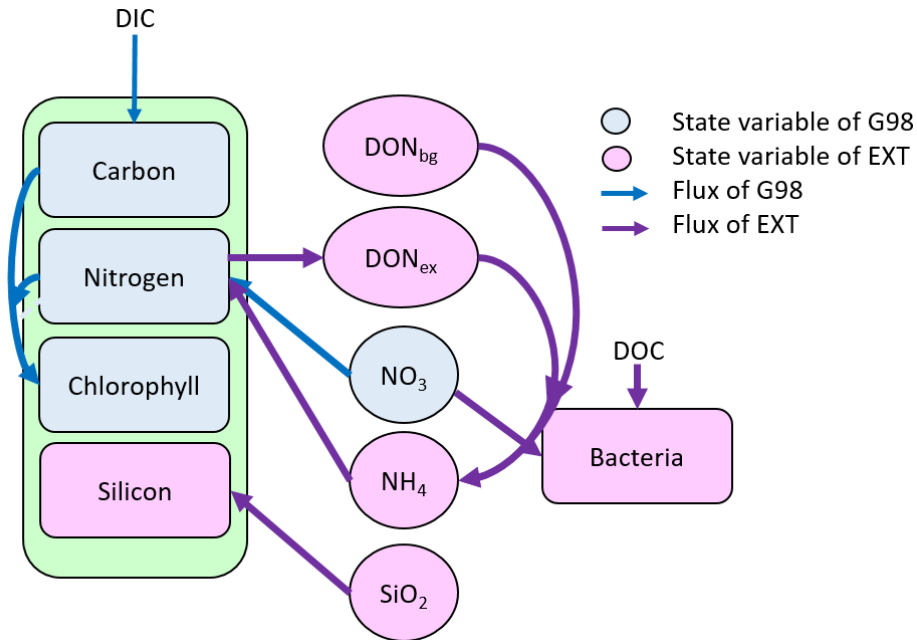
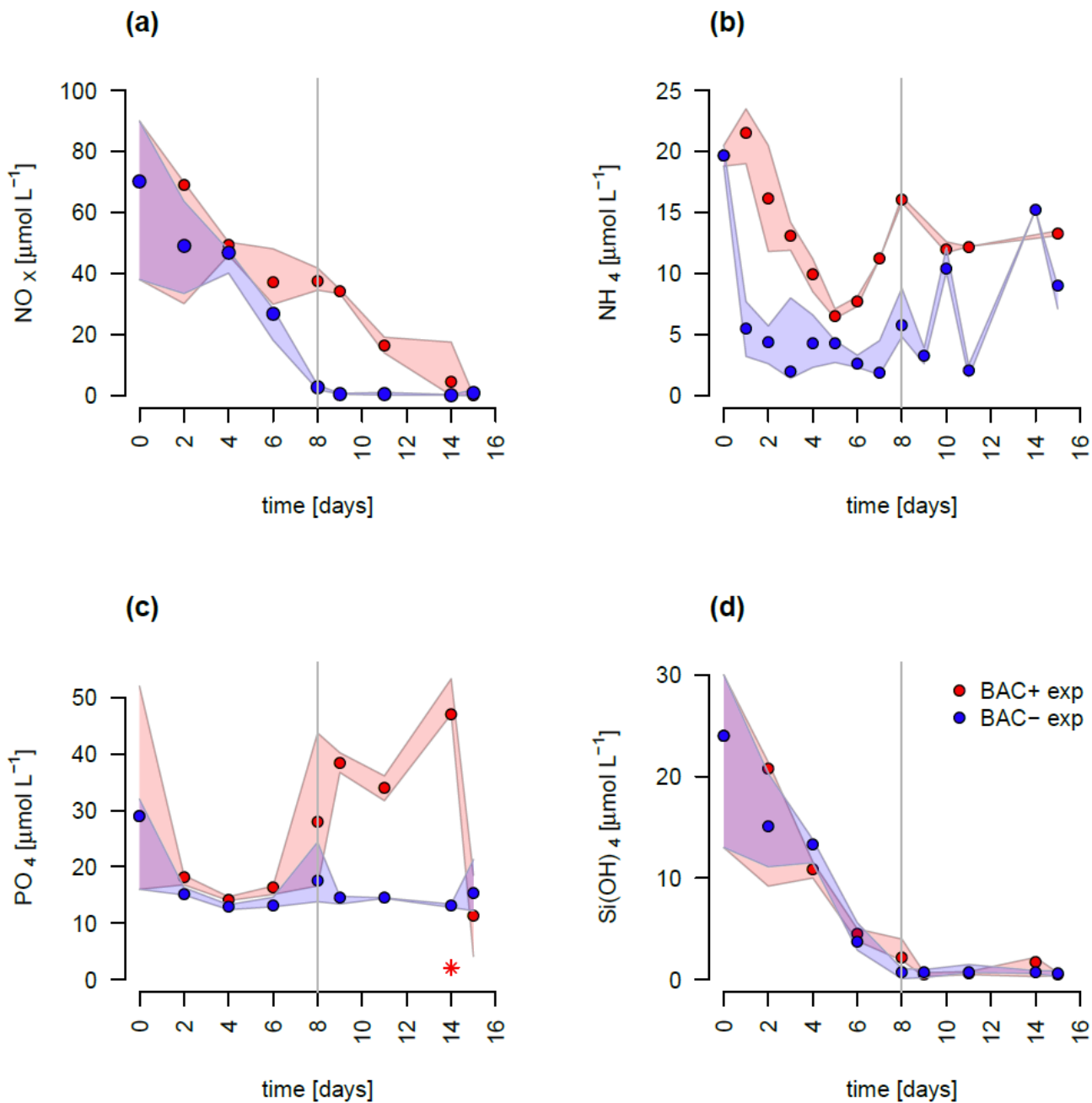


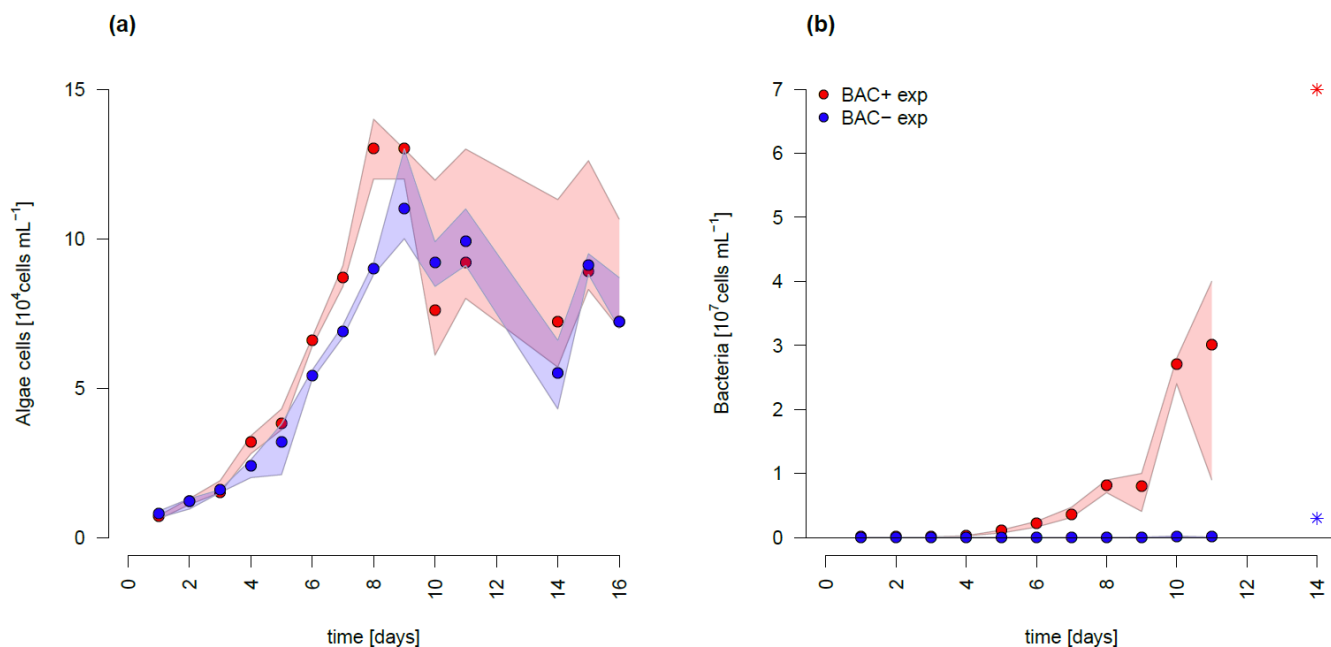
Figure 1. Schematic representation of the state variables and connections and controls in the G98 model (blue) and EXT model (purple). The EXT model has the same formulations as G98 with the additions shown in purple.



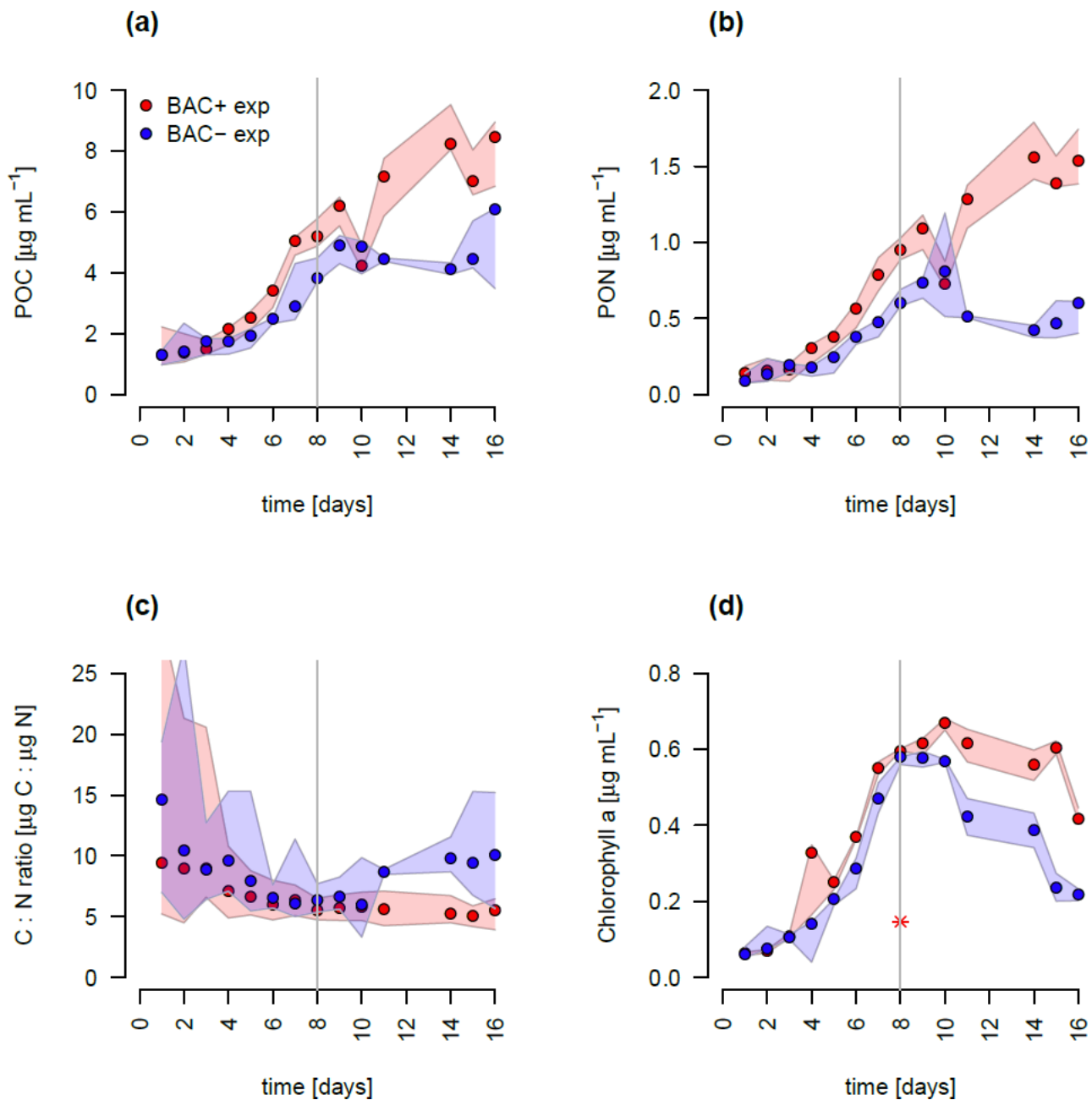
1005

Figure 2. Nutrient measurements over the experimental incubations of a) NO_x , ($\text{NO}_3^- + \text{NO}_2^-$) b) NH_4^+ , c) PO_4^{2-} (The asterisk indicates a presumed measurement error), d) Silicate, blue circles are BAC- cultures and red symbols are BAC+ cultures. Circles show median values (blue = BAC-, red = BAC+) and the colored polygons show maximum and minimum of measured data (n=1-3, Table S2). The grey line shows the beginning of the stationary growth phase of *Chaetoceros socialis*.

1010

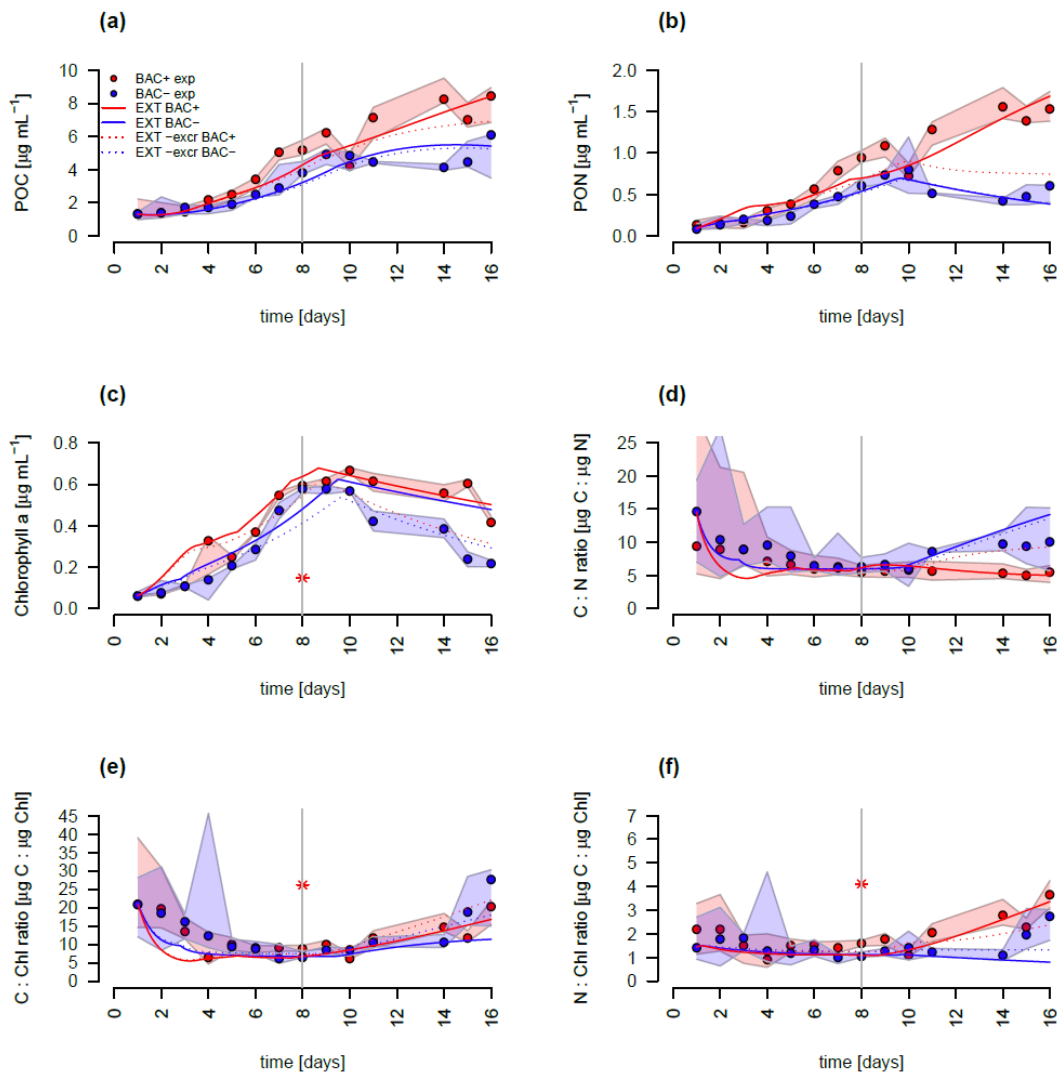


1015 Figure 3. Abundances of a) *Chaetoceros socialis* and b) bacteria over the 14 day experimental period. Blue data are from BAC- cultures and red from BAC+ cultures. The asterisks at day 14 indicate potential outliers as based on only one replicate. Circles represent median values (blue= BAC-, red = BAC+) and the colored polygons show maximum and minimum of measured data (n=1-3, Table S2, Not visible for bacteria counts in BAC- cultures due to very small range). The maximum values of the BAC+ experiment includes algae cells in the biofilm (after day 9).



1020 Figure 4. Total particulate organic a) Carbon (POC) b) Nitrogen (PON), c) C : N ratios, and d)
 Chlorophyll a concentration in experimental cultures (The asterisk indicates a presumed measurement
 error). Blue symbols are BAC- cultures and red show BAC+ cultures. Circles show median values (blue
 = BAC-, red = BAC+) and the colored polygons show the maximum and minimum of measured data
 (n=2-3, Table S2). The grey line indicates the start of the stationary phase.

1025



1030 Figure 5. Model fit of the EXT model to the BAC- (blue) and BAC+ (red) experiment. Circles show
 1035 median values and the colored polygons show the maximum and minimum of measured data (n=2-3,
 Table S2). Solid lines show the model outputs of a) POC, b) PON, c) Chl (The asterisk indicates a
 presumed measurement error) , d) C:N, e) C:Chl, and f) N:Chl. Dotted lines show the model fit without
 additional Carbon excretion term x_f . At day 8 the threshold for silicate limitation is reached leading to
 reduced photosynthesis (by the factor given by S_{iPS}) and inhibited Chl synthesis, which is visible as
 sharp transitions in POC and Chl.

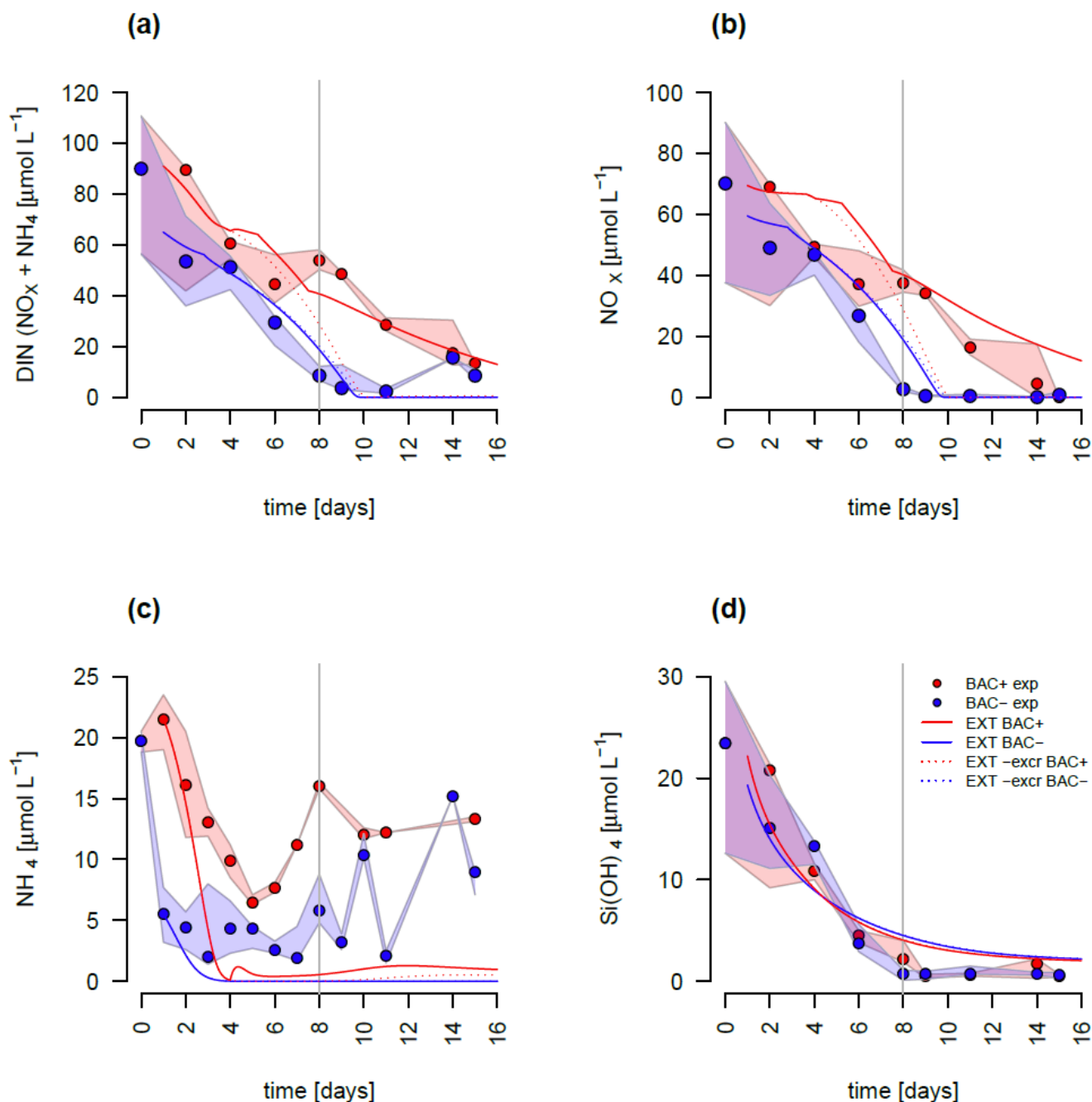


Figure 6. Model fit of the EXT model to the BAC- (blue) and BAC+ (red) experiment. Circles show median values and the colored polygons show the maximum and minimum of measured data (n=1-3, Table S2). Solid lines show the model outputs of a) DIN (NO_x and NH₄), b) NO_x, c) NH₄, and d) Si(OH)₄ (All model fits overlap).

1040

Table

- 1045 Table 1. A comparison of major components contributing to the complexity of different models discussed. #param is the number of parameters. In case of ecosystem models (SINMOD, BFM, MEDUSA, LANL, NEMURO, NPZD only the model formulations representing the components of the current model (phytoplankton growth, remineralisation, nutrient dynamics) are considered. For the full ecosystem scale models we give the original reference to the biogeochemical compartment of the
- 1050 ecosystem scale models and examples for more recent versions with updated formulations of other model compartments (e.g. physical drivers). REM designates those models that include Remineralisation (Rem) marked with V is present and X is absent. Ratios shows if the stoichiometry in the model considers variable or fixed ratios of intracellular elements (C:N:Si:P:Fe). The Nutrients considered are given under Nutrients. If DIN is considered as both NH₄ and NO₃, N is shown as N².
- 1055 MEDUSA has Fe dependent Si:N ratios, which makes them fixed in the Arctic (fixed*).

Model	Reference	#param	Rem	ratios	Nutrients
Culture scale					
EXT	This study	21 ^{*1}	V	variable	N ² , Si
G98	Geider et al., 1998	10 ^{*2}	X	variable	N
ANIM	Flynn, 1997	30	V	variable	N ²
SHANIM	Flynn and Fasham, 1997	23	X	variable	N ²
Flynn01	Flynn, 2001	54	X	variable	N ² , Si, P, Fe
Flynn18	Flynn et al., 2018	27	X	variable	N
Ecosystem scale					
BFM	Vichi et al., 2007	54	V	variable	N ² , Si, P, Fe
BFM17	Smith et al., 2020	24	V	variable	N ² , P
REcoM-2	Hauck et al., 2013	28	X	variable	N, Si, Fe
	Schourup-Kristensen et al. 2018				
MEDUSA	Yool and Popova, 2011	21	V	fixed*	N, Si, Fe
	Henson et al., 2018				
LANL	Moore et al., 2004	15	V	fixed	N ² , Si, P, Fe
NEMURO	Kishi et al., 2007	21	V	fixed	N ² , Si
	Amju et al., 2020				
NPZD	Gruber et al., 2006	9	V	fixed	N ²
SINMOD	Wassmann et al., 2006	12	X	fixed	N ² , Si
	Alver et al., 2016				

Degrees of freedom after constraints by the measured data are ^{*1}14 and ^{*2}6

1060 **Appendix****Tables**

Table A1. State variables of the G98 model and the EXT model (marked with V if present and X if absent) with units and designation if these state variables had been measured in the experiment.

variable	Description	G98	EXT	Measured	Unit
DIN	Dissolved inorganic nitrogen	V	V	V	mgN m ⁻³
C	Particulate organic carbon	V	V	V	mgC L ⁻¹
N	Particulate Nitrogen	V	V	V	mgN L ⁻¹
Chl	Chlorophyll a	V	V	V	mgChl L ⁻¹
Si _d	Dissolved Silicate	X	V	X	μmol L ⁻¹
Si _p	Particulate/biogenic Silicon	X	V	V	mgSi L ⁻¹
Bact	Bacteria cells	X	V	V	mgC _{bac} L ⁻¹
DOC	Dissolved organic carbon	X	V	V	mgC L ⁻¹
DON _r	refractory dissolved organic nitrogen	X	V	X	mgN L ⁻¹
DON _l	labile dissolved organic nitrogen	X	V	X	mgN L ⁻¹
NH ₄	Ammonium	X	V	V	μmol L ⁻¹
NO ₃	Nitrate	X	V	V	μmol L ⁻¹
Q	Particulate N : C ratio	X	V	X	gN gC ⁻¹
θ ^C	Chl to POC ratio	X	V	X	gChl gC ⁻¹
θ ^N	Chl : phytoplankton nitrogen ratio	X	V	X	gChl gN ⁻¹

1065

1070

Table A2. Parameters of the original G98 model and the model extension with associated units.

parameter		Unit
G98		
ζ	cost of biosynthesis	gC gN ⁻¹
R ^C	The carbon-based maintenance metabolic rate	d ⁻¹
θ_{\max}^N	Maximum value of Chl:N ratio	gChl gN ⁻¹
Q _{min}	Min. N:C ratio	gN gC ⁻¹
Q _{max}	Max. N:C ratio	gN gC ⁻¹
α^{Chl}	Chl-specific initial C assimilation rate	gC m ² (gChl $\mu\text{mol photons}$) ⁻¹
I	Incident scalar irradiance	$\mu\text{mol photons s}^{-1} \text{m}^{-2}$
n	Shape factor for V ^N _{max} max photosynthesis	-
K _{no3}	Half saturation constant for nitrate uptake	$\mu\text{mol L}^{-1}$
P ^C _{ref}	Value of max C specific rate of photosynthesis'	d ⁻¹
Extension		
x _f	Carbon excretion fraction	-
K _{si}	Half saturation constant for Si uptake	$\mu\text{mol L}^{-1}$
V _{max}	maximum Si uptake rate	$\mu\text{mol Si d}^{-1} \text{mg C}^{-1}$
s _{min}	minimum Si required for uptake	$\mu\text{mol L}^{-1}$
rem	remineralisation rate of excreted don	mgC _{bac} ⁻¹ d ⁻¹
rem _d	remineralisation rate of refractory don	mgC _{bac} ⁻¹ d ⁻¹
μ_{bact}	bacteria growth rate	mgC _{bac} L ⁻¹ d ⁻¹
bact _{max}	Carrying capacity for bacteria	mgC _{bac} L ⁻¹
K _{nh4}	Half saturation constant for ammonium uptake	$\mu\text{mol L}^{-1}$
nh4 _{thres}	threshold concentration for ammonium uptake	$\mu\text{mol L}^{-1}$
S _{ips}	Fraction of photosynthesis possible after Si lim.	-
Constants		
RR	Redfield ratio	molC molN ⁻¹
M _N	Molar mass of nitrogen	g mol ⁻¹

Table A3. Parameters and constants of the original G98 model and the EXT model with initial values used in the model and the lower and upper value constraints used for model fitting, unless the parameter was already defined by the data (measured). The constraints are either based on G98 fits to other diatom species, to present experimental data, or to typical values found in the literature.

parameter	value	lower	upper	constrained by
G98				
ζ	1	1	2	G98
R^C	0.096	0.01	0.1	G98
θ_{\max}^N	1.7	measured		Data
Q_{\min}	0.05	measured		Data
Q_{\max}	0.3	measured		Data
α^{Chl}	0.049	0.075	1	G98
I	100	measured		Data
n	2.572	1	4	G98
K_{no3}	1	1	10	G98
P_{ref}^C	0.8	0.5	3.5	G98
Extension				
x_f	0.0546	0.01	0.3	Schartau et al., 2017
K_{si}	7.6	0.5	8	Werner 1978
V_{\max}	0.1	0.05	0.9	Data
s_{\min}	1.82	1.5	6	Werner 1978
rem	5.391	0.1	10	open (rem > rem _d)
rem _d	0.00066	0.0001	0.1	open (rem _d < rem)
μ_{bact}	0.8	0.01	0.8	Data
bact _{max}	0.7	0.1	1	Data
K_{nh4}	4.537	0.5	9.3	Eppley 1969
nh4 _{thres}	0.486	0.1	10	open
S _{ips}	0.6	0.01	0.7	Werner 1978
Constants				
RR	6.625	constant		Redfield 1934
M_N	14	constant		Periodic table

Table A4. Output of the sensitivity analysis (senFun of the FME package in R, EXT fit on BACT+) with the value for each parameter and different sensitivity indices obtained after quantifying the effects of small perturbations of the parameters on the output variables (POC, PON, Chl, DIN). The L1 and L2

norms are normalized sensitivity indices defined as $L1 = \sum \frac{|S_{i,j}|}{n}$ and $L2 = \sqrt{\frac{S_{i,j}^2}{n}}$ with $S_{i,j}$ being the the

1090 sensitivity of parameter i for model output j.

par	value	L1	L2
G98			
ζ	1.00	0.18	0.30
R^C	0.096	0.60	0.80
θ_{\max}^N	1.70	0.37	0.52
Q_{\min}	0.05	0.05	0.06
Q_{\max}	0.30	0.36	0.62
α^{Chl}	0.05	0.27	0.43
I	100	0.27	0.43
n	2.572	0.53	0.96
K_{no3}	1.00	0.007	0.015
P_{ref}^C	0.80	1.27	2.05
EXT			
x_f	0.0546	0.17	0.24
K_{si}	7.6	0.00	0.00
V_{\max}	0.1	0.00	0.00
s_{\min}	1.82	0.00	0.00
rem	5.391	0.005	0.007
rem _d	0.00065	0.09	0.21
μ_{bact}	0.8	0.18	0.36
bact _{max}	0.7	0.04	0.117
K_{nh4}	4.5372	0.06	0.08
nh4 _{thres}	0.4863	0.00	0.00
S _{ips}	0.6	0.07	0.18

Table A5. Other parameters calculated and used in the model equations

parameter	Description	Unit
P^C_{phot}	C-specific rate of photosynthesis	d^{-1}
P^C_{max}	Maximum value of P^C_{phot} at temperature T	d^{-1}
R^{Chl}	Chl degradation rate constant	d^{-1}
R^{N}	N remineralization rate constant	d^{-1}
$V^{\text{C}}_{\text{nit}}$	Diatom carbon specific nitrate uptake rate	gN (gC d)^{-1}
$V^{\text{C}}_{\text{ref}}$	Value of $V^{\text{C}}_{\text{max}}$ at temperature T	gN (gC d)^{-1}
p_{Chl}	Chl synthesis regulation term	-
μ	specific growth rate of algae	cells d^{-1}

1100

1105

1110

1115

1120

Table A6. Model equations from G98 (Geider et al., 1998) corrected for typographical errors by Ross and Geider (2009) with extensions.

1)	Carbon synthesis (C originates from unmodelled excess pool of DIC)	$\frac{dC}{dt} = (P^C - \zeta V_N^C - R^C)C = \mu C$
2)	Chl synthesis	$\frac{dChl}{dt} = \left(\frac{\rho^{chl} V_N^C}{\Theta^C} - R^{chl} \right) Chl$
3)	Nitrogen uptake	$\frac{dN}{dt} = \left(\frac{V_N^C}{Q} - R^N \right) N$
4)	from Eq. (1) and (2)	$\frac{dQ}{dt} = V_N^C - \mu Q$
5)	from Eq. (1) and (2)	$\frac{d\Theta^C}{dt} = V_N^C \rho^{chl} - \Theta^C \mu$
6)	Photosynthesis	$P^C = P_{max}^C \left[1 - \exp\left(-\frac{I}{I_K}\right) \right]$
7)	Max. N uptake	$V_N^C = V_{ref}^C \left[\frac{Q_{max} - Q}{Q_{max} - Q_{min}} \right] \frac{DIN}{DIN + K_{no3}}$
8)	with	$\rho^{chl} = \Theta_{max}^N \left[1 - \exp\left(-\frac{I}{I_K}\right) \right]$
9)		$V_{ref}^C = P_{ref}^C Q_{max}$
10)		$P_{max}^C = P_{ref}^C \frac{Q - Q_{min}}{Q_{max} - Q_{min}}$
11)		$I_K = \frac{P_{max}^C}{\alpha^{chl} \Theta^C}$

1130 Table A7. Model equations of the EXT model based on G98

1a)	Carbon synthesis (<i>Reduced C synthesis under Si limitation after Werner 1978</i>)	$IF (Si_d < 2 s_{min})$ $Si_{PS} = Si_{PS}$ $ELSE$ $Si_{PS} = 1$
1b)		$\frac{dC}{dt} = Si_{PS}(P^C - \zeta V_N^C - R^C - xf)C = \mu C$
2)	Chl synthesis (<i>Chl synthesis stops under Si limitation after Werner 1978</i>)	$IF (Si_d < 2 s_{min})$ $\frac{dChl}{dt} = -R_{Chl} Chl$ $ELSE$ $\frac{dChl}{dt} = \left(\frac{\rho_{Chl} V_N^C}{\Theta^C} - R_{Chl} \right) Chl$
3)	from Eq. (1 & 2)	$\frac{dQ}{dt} = V_N^C - \mu Q$
4)	from Eq. (1 & 2)	$\frac{d\Theta^C}{dt} = V_N^C \rho_{Chl} - \Theta^C \mu$
5)	Nitrogen uptake	$\frac{dN}{dt} = \left(\frac{V_N^C}{Q} - R^N - xf \right) N$
6)	Bacteria biomass production (<i>Logistic growth</i>)	$\frac{dBact}{dt} = Bact \mu_{Bact} \left(1 - \frac{Bact}{Bact_{max}} \right)$
7a)	Silicate uptake (<i>Monod kinetics after Spilling et al., 2010</i>)	$\frac{dSi_d}{dt} = V_S^C = \left(V_{max} Si_d \frac{Si_d - S_{min}}{K_{si} S_{min}} \right) C$

7b)

$$\frac{dSi_p}{dt} = -\frac{dSi_d}{dt} \quad 14$$

8) Ammonium uptake and production

$$IF \left(\frac{C}{N} < 10 \right)$$

(Threshold after Tezuka 1989, and Gilpin 2004)

$$\frac{dNH4}{dt} = \frac{-\left(\frac{V_{NH4}^C}{Q}\right)N + Bact\ DONl\ rem + Bact\ DONr\ rem_d}{M_N\ 10^3}$$

ELSE IF ($NH4 > nh4_{thresj}$)

$$\frac{dNH4}{dt} = \frac{-\left(\frac{V_{NH4}^C}{Q}\right)N - \frac{dBact}{dt}RR}{M_N\ 10^3}$$

ELSE

$$\frac{dNH4}{dt} = \frac{-\left(\frac{V_{NH4}^C}{Q}\right)N}{M_N\ 10^3}$$

9) DON uptake and production

$$IF \left(\frac{C}{N} < 10 \right)$$

$$\frac{dDONl}{dt} = \frac{-Bact\ DONl\ rem + xf\ N - \frac{dBact}{dt}RR}{M_N\ 10^3}$$

$$\frac{dDONr}{dt} = \frac{-Bact\ DONr\ rem_d}{M_N\ 10^3}$$

ELSE

$$\frac{dDONl}{dt} = \frac{xf\ N}{M_N\ 10^3}$$

$$\frac{dDONr}{dt} = 0$$

10) DIN uptake

$IF (NH4 > nh4_{thresh})$

$$\frac{dDIN}{dt} = \frac{-\left(\frac{V_{NO3}^C}{Q}\right)N}{M_N 10^3}$$

ELSE

$$\frac{dDIN}{dt} = \frac{-0.2 \left(\frac{V_{NO3}^C}{Q}\right)N - \frac{dBact}{dt} RR}{M_N 10^3}$$

11) Photosynthesis

$$P^C = P_{max}^C \left[1 - \exp\left(-\frac{I}{I_K}\right)\right]$$

12a) Max NO3 uptake

$$V_{NO3}^C = V_{ref}^C \left[\frac{Q_{max} - Q}{Q_{max} - Q_{min}}\right] \frac{NO3}{NO3 + K_{no3}}$$

12b) Max NH4 uptake

$$V_{NH4}^C = (0.01 Q) 0.0021 \frac{NH4}{NH4 + K_{nh4}}$$

*(based on SHANIM
Eq4 by Flynn and
Fasham, 1997)*

13) Max N uptake

$IF (NH4 > nh4_{thresh})$

*(Based on Flynn and
Fasham, 1997 and
Flynn, 1999 showing no
total inhibition in cold
water)*

$$V_N^C = V_{NH4}^C + 0.2 V_{NO3}^C$$

ELSE

$$V_N^C = V_{NH4}^C + V_{NO3}^C$$

14) with

$$\rho^{chl} = \Theta_{max}^N \left[1 - \exp\left(-\frac{I}{I_K}\right)\right]$$

15)

$$V_{ref}^C = P_{ref}^C Q_{max}$$

16)

$$P_{max}^C = P_{ref}^C \frac{Q - Q_{min}}{Q_{max} - Q_{min}}$$

17)

$$I_K = \frac{P_{max}^C}{\alpha^{chl} \Theta^C}$$

18) DOC to DONr
conversion

$$DONr = \frac{DOC}{RR}$$

1135

1140

1145

1150

Table A8. Output of the collinearity or parameter identifiability analysis using the collin function (G98 fit on BACT- data) of the FME R package (Soetart et al., 2010b). A subset of any combinations of two parameter with a collinearity above 20, indicating non-identifiable parameter combinations is given (Brun et al., 2001). Parameter combinations tested are marked with a V in the left part of the table, the collinearity output is given on the right site.

1155

Parameter combinations										collinearity
ζ	R^C	θ_{\max}^N	Q_{\min}	Q_{\max}	α^{Chl}	I	n	K_{no3}	P_{ref}^C	
V	X	V	X	X	X	X	X	X	X	27
V	X	X	X	V	X	X	X	X	X	98
V	X	X	X	X	V	X	X	X	X	31
V	X	X	X	X	X	V	X	X	X	31
V	X	X	X	X	X	X	V	X	X	93
X	V	X	X	X	X	X	X	X	V	25
X	X	V	X	V	X	X	X	X	X	34
X	X	V	X	X	V	X	X	X	X	101
X	X	V	X	X	X	V	X	X	X	101
X	X	V	X	X	X	X	V	X	X	38
X	X	V	X	X	X	X	X	X	V	32
X	X	X	X	V	V	X	X	X	X	40
X	X	X	X	V	X	V	X	X	X	40
X	X	X	X	V	X	X	V	X	X	146
X	X	X	X	X	V	V	X	X	X	455473
X	X	X	X	X	V	X	V	X	X	46
X	X	X	X	X	V	X	X	X	V	28
X	X	X	X	X	X	V	V	X	X	46
X	X	X	X	X	X	V	X	X	V	28

1160

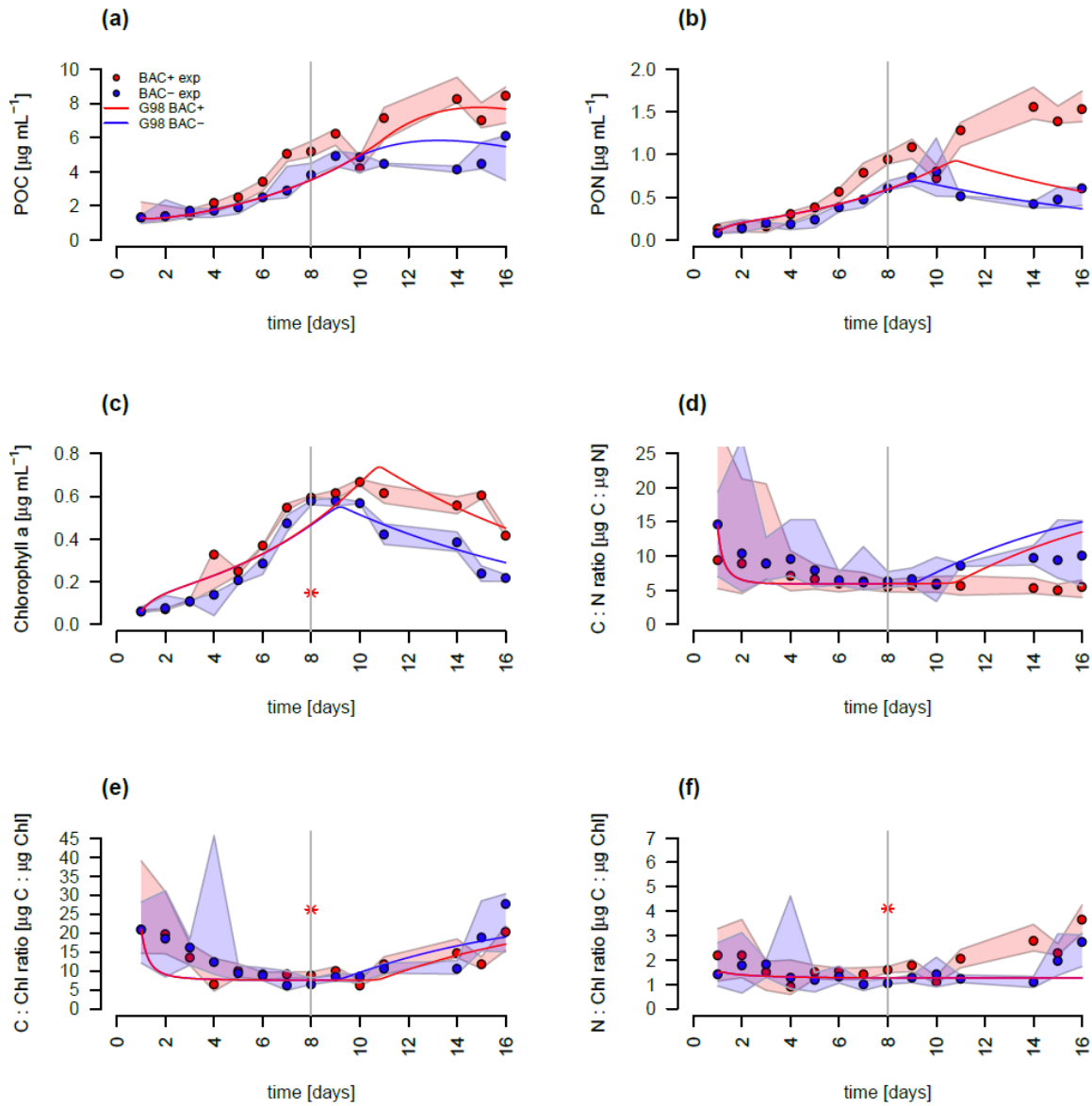


Figure B1: Model fit of the G98 model to the BAC- (blue) and BAC+ (red) experiment. Circles show median values and the colored polygons show the minimum and maximum of the measured data (n=2-3, Table S2). Solid lines show the model outputs of a) POC, b) PON, c) Chl (The asterisk indicates a presumed measurement error), d) C:N, e) C:Chl, and f) N:Chl.

Equations

Equation C1. F-ratio estimation in the cultivation experiments with the average PON concentrations at day 13 to 15 (PON^{d13-15}) for the BAC- and BAC+ treatments.

$$f - ratio = \frac{PON_{BAC-}^{d13-15}}{PON_{BAC-}^{d13-15} + PON_{BAC+}^{d13-15}}$$

1175

Equation C2. normalized RMSE with i being the different variables (POC, PON, Chl, DIN), and j the different values of each state variable. Predicted values are given as P and observed values as O.

$$RMSE = \sqrt{\sum_{i=1}^{n,p} \sum_{j=1}^{p} \frac{(P_{i,j} - O_{i,j})^2}{Var(O_i)}}$$

1180

1185

1190

1195

1200

1205